



A new method to characterize the nonlinear magneto-viscoelasticity behavior of magneto-active elastomers under large amplitude oscillatory axial (LAOA) loading

Hossein Vatandoost · Ramin Sedaghati · Subhash Rakheja

Received: 16 January 2023 / Accepted: 6 December 2023 / Published online: 17 January 2024
© Crown 2024

Abstract The nonlinear viscoelasticity of magneto-active elastomers (MAEs) under large amplitude oscillatory shear (LAOS) loading has been extensively characterized. A reliable and effective methodology, however, is lacking for such characterizations under large amplitude oscillatory axial (LAOA) loading. This is partly due to complexities associated with experimental compression mode characterizations of MAEs and in-part due to their asymmetric stress–strain behavior leading to different elastic moduli during extension and compression. This study proposes a set of new nonlinear measures to characterize nonlinear and asymmetric behavior of MAEs subject to LAOA loading. These include differential large/zero strain moduli and large/zero strain-rate viscosity, which could also facilitate physical interpretations of the inter- and intra-cycle nonlinearities observed in asymmetric and hysteretic stress–strain responses. The compression mode stress–strain behavior of MAEs was experimentally characterized under different magnitudes of axial strain (0.025 to 0.20), strain rate (frequency up to 30 Hz) and magnetic flux density (0 to 750mT). The measured stress–strain responses were decomposed into elastic, viscous and viscoelastic stress components using Chebyshev polynomials and

Fourier series. The stress decomposition based on Chebyshev polynomials permitted determination of equivalent nonlinear elastic and viscous stress components, upon which the proposed measures were obtained. An equivalent set of Fourier coefficients was also obtained for estimating equivalent elastic/viscous stress, thereby facilitating faster calculation of the proposed material measures. The proposed methodology is considered to serve as an effective tool for deriving constitutive models for describing nonlinear and asymmetric characteristics of MAEs.

Keywords Magneto-active materials · Nonlinear viscoelasticity · Asymmetric stress–strain behavior · Large amplitude oscillatory axial (LAOA) loading · Differential large/zero strain modulus · Differential large/zero strain-rate viscosity

1 Introduction

The noise and isolation performance of conventional passive elastomers including natural and silicone rubbers, widely used in the automotive and civil engineering sectors, is generally limited to a narrow band frequency range. Adaptive elastomers, particularly the magneto-active elastomers (MAEs) with tuneable properties, are considered promising alternatives not only for noise and vibration control but also

H. Vatandoost (✉) · R. Sedaghati · S. Rakheja
Department of Mechanical, Industrial, and Aerospace
Engineering, Concordia University, Montreal,
QC H3G 1M8, Canada
e-mail: h_vatand@encs.concordia.ca

for many other engineering applications such as soft robotics and programmable actuations [1, 2]. More specifically, MAEs exhibit rapid, continuous and reversible response to an external magnetic field, which makes them well-suited for adaptive noise/vibration isolations, large-scale shape transformations [3] and controllable actuations [4]. MAEs comprise two primary components: (i) magnetically soft (i.e., carbonyl iron particles), hard (i.e., neodymium iron boron-NdFeB [5]) or combination of soft and hard particles [6]; and (ii) non-magnetic medium (i.e., silicone rubbers). Compared to their counterpart in liquid state, namely magneto-rheological (MR) fluids (MRFs), which exhibit field-dependent yield stress [7] and apparent viscosity [8] (field-dependent damping), MAEs exhibit field-dependent modulus [9], which makes them ideal materials for development of adaptive devices (i.e., tuneable vibration isolators). Understanding the characteristics of MAEs, including identification of their field- and load-dependent moduli, is a fundamental requirement. This characterization is important for realizing optimal designs of MAE-based adaptive intelligent devices and developing effective models and controller syntheses.

MAEs can operate in shear [10] as well as extension/compression mode [11–13]. Shear mode characterization of MAEs in linear and nonlinear regimes (i.e., large amplitude oscillatory shear (LAOS) loadings) have been extensively investigated (e.g., [10, 14, 15]), while relatively fewer studies have explored their compression/extension mode properties, although the MAEs exhibit substantially higher MR effect in the compression/extension mode [16–19]. This is likely due to ease of experimental characterizations in the shear mode, where the magnetic field is applied in a direction normal to the mechanical loading. Magneto-mechanical properties of MAEs in the shear mode are thus well understood under various design and operational factors. These include: properties of the matrix material; size, type, concentration, and spatial distribution of ferromagnetic particles [20]; and broad ranges of mechanical and magnetic loading conditions [14, 15]. Axial mode (i.e., compression/extension) characterization of an MAE imposes considerable challenges since it involves applications of mechanical and magnetic loading in the same direction. The experimental characterizations thus require decoupling of magnetic force from viscoelastic force of the MAE [21, 22]. The

lack of a reliable and accurate decoupling methodology together with an electromagnetic module that permits unidirectional magnetic and mechanical loadings are likely the primary reasons for relatively fewer efforts on axial mode characterizations of MAEs. The decoupling also demands for accounting of the actual sample form [23], related to demagnetizing factor [24], and shape of magnetizable particles [25].

In the shear mode, MAEs generally exhibit symmetric stress–strain characteristics even under LAOS loading, which has facilitated identifications of field-dependent moduli. First harmonic storage and loss moduli (G'_1 and G''_1), derived from Fourier transform of the stress response, are effectively being used to characterize viscoelastic properties in the linear regime. The first harmonic moduli have also been used to estimate dynamic response characteristics of viscoelastic materials in the nonlinear regime (i.e., LAOS) [26, 27]. This approach, however, cannot accurately describe the effects of nonlinearities attributed to strain softening, strain stiffening [28], rate-dependent hysteresis, etc. Owing to existence of only odd harmonics in shear mode due to symmetric stress–strain response, Cho et al. [29] proposed a stress-decomposition (SD) technique, also referred to as geometrical interpretation, to decompose the stress response into elastic and viscous components using either a search technique or polynomial regression functions. The method permitted more accurate characterizations of nonlinear viscoelasticity under LAOS by analyzing relative contributions of the elastic and viscous stress components to the total nonlinear stress response. While the proposed methodology permitted geometrical interpretations of viscoelastic materials subject to LAOS, the identified storage and loss moduli were not unique and showed dependence on the order of the polynomial function. Ewoldt et al. [30, 31] developed a complete framework to uniquely quantify viscoelastic material moduli under LAOS on the basis of Chebyshev polynomial functions, which permitted unique physical interpretations of local nonlinearities (e.g., intra-cycle strain stiffening). The study proposed the use of minimum and maximum strain moduli to describe nonlinear viscoelastic responses of the material subject to LAOS. Owing to orthogonality of the Chebyshev polynomials, unlike the polynomial-based SD reported in [28], the resulting material constants were truncated-independent, and thus unique.

Unlike the shear mode, the viscoelastic materials exhibit asymmetric stress–strain behavior in the axial mode (i.e., compression/extension), especially under large amplitude oscillatory axial (LAOA) loading, which yields the presence of even- as well as odd-harmonics in the stress response. The magneto-active materials exhibit even greater asymmetry in the stress response due to additional asymmetric variations in the applied magnetic field [21, 32]. MAEs show inherent nonlinear tension–compression asymmetry even at relatively small macroscopic strain (2–5%) due to different particle–particle interactions and particle chain microstructure during compression and extension [33, 34]. The local measures of moduli during compression and extension may thus differ. Only limited investigations of response behaviors of viscoelastic materials subject to LAOA loading, however, could be found [35–39]. Moreover, these conventional methods do not quantify nonlinear stress responses during the compression and extension cycles. For instance, Kim et al. [35] investigated the asymmetric response of a highly shear-thinning viscoelastic material subjected to LAOA using the SD method together with non-orthogonal polynomial fitting. It was deduced that the asymmetry in the response was originated from elastic contribution to the normal stress [38]. Yu et al. [40] developed a general SD methodology for evaluating materials' responses to LAOS, which incorporated both odd as well as even-harmonics, although using non-orthogonal polynomials. Ewoldt [30] provided some interpretations relevant to contributions of even harmonics using the minimum and maximum strain moduli, as a final touch in the framework developed for stress response analyses for LAOS. The large nonlinearities observed in the response near extremities of the compression and extension cycles (e.g., up-turn or down-turn [34]), however, could not be accurately quantified. Besides, the method presented in [30] realized two different values for the minimum strain moduli, thereby not providing a unique interpretation.

To the best of our knowledge, identifications of viscoelastic material moduli of MAEs subject to LAOA loading have not yet been attempted. This study proposes alternate measures to characterize nonlinear response characteristics of MAEs subject to LAOA loading. These include: (i) the differential large strain modulus and differential large strain-rate viscosity and (ii) the differential zero strain modulus and

differential zero strain-rate viscosity. For this purpose, several MAE samples were fabricated, and a series of experiments were performed to characterize their magneto-mechanical behavior under a range of LAOA loading. The stress response was subsequently estimated using Fourier series and Chebyshev polynomials, thereby decomposing into elastic, viscous, and viscoelastic stress components. The SD based on Chebyshev polynomials permitted calculation of equivalent nonlinear elastic and viscous stresses, thereby determining the large/zero strain elastic moduli, together with the large/zero strain-rate viscosity. Unlike the slope of loading/unloading paths of the total stress, the proposed measures, are deliberately chosen as the slope of the equivalent nonlinear elastic, and viscous stress components, such that not only they possess unique values but also both can converge to the linear strain-independent elastic modulus/dynamic viscosity under relatively small strains. It should be highlighted that the presented method to obtain differential moduli from the slope of equivalent elastic/viscous stress has also rarely been investigated in LAOS (i.e., Yao et al. [41]) and few studies have quantified nonlinearity in LAOS by deriving differential moduli from the total stress [42, 43]. In the present work, an equivalent set of Fourier coefficients was also obtained for estimating the equivalent elastic/viscous stress, which facilitates the calculation process of the suggested material measures. The proposed measures can also interpret inter-cycle (e.g., strain amplitude softening/stiffening) and intra-cycle (e.g., strain stiffening) nonlinearities of MAEs under LAOA loadings.

2 Experiment

2.1 Material and methods

Several batches of unaligned and aligned MAEs were fabricated in the laboratory by mixing magnetically soft carbonyl iron particles with Eco-flex 0020 silicone rubber (Smooth-ON Inc., USA) using the process described in [32]. The particles were magnetically soft (type SQ) with approximately spherical shape with diameter ranging from 2 to 5 μm (BASF Co., Germany). The MAE samples were fabricated with 30% volume fraction of iron particles. The unaligned MAE batches were cured in the ambient

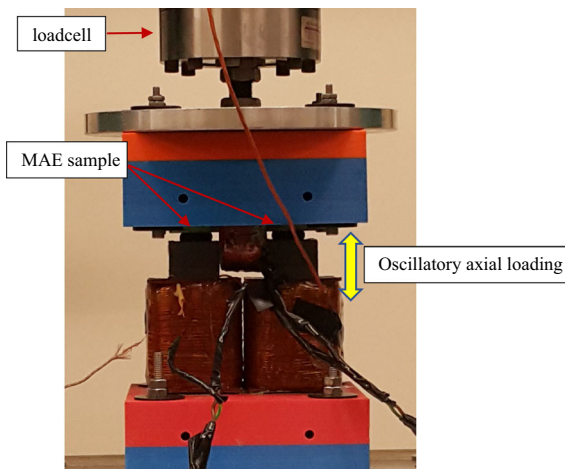


Fig. 1 Experimental characterizations of MAE samples under large amplitude oscillatory axial (LAOA) loading

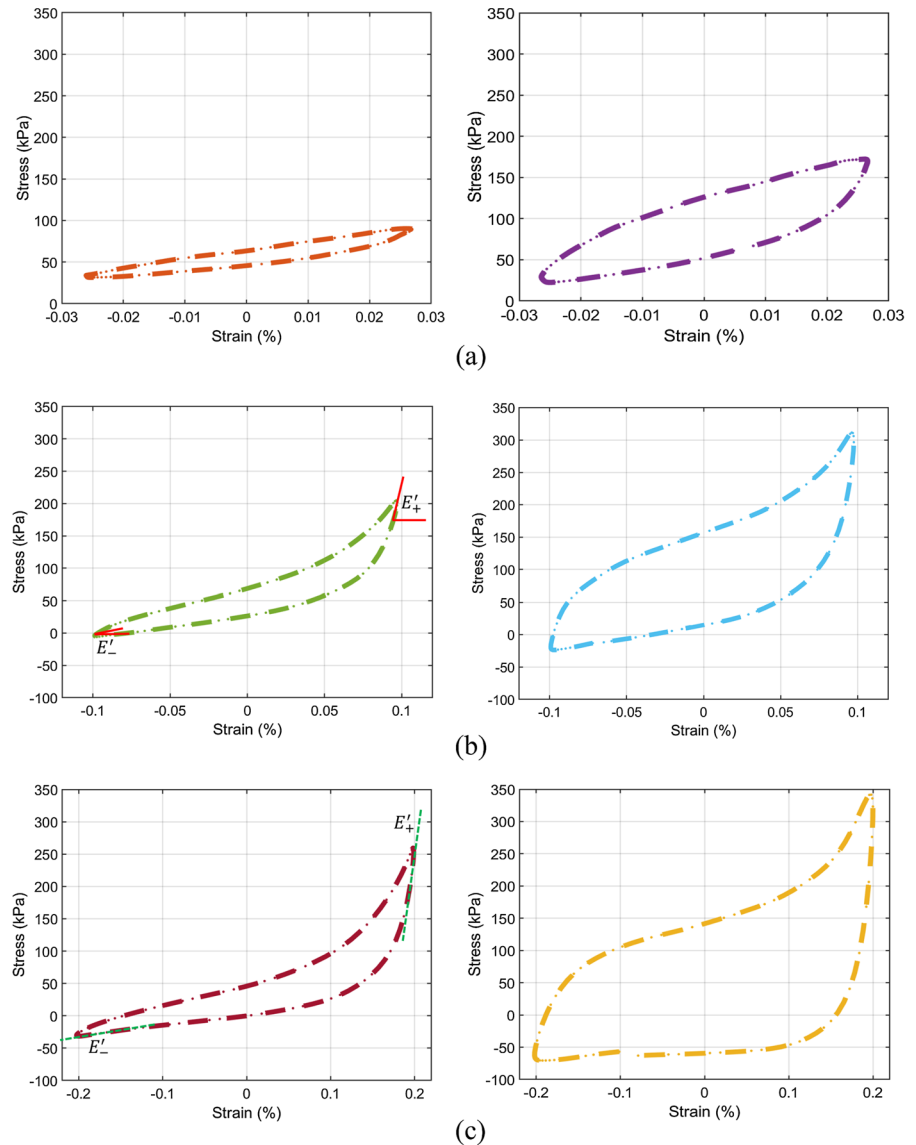
laboratory condition for 24 h, while the aligned MAE batches were cured under external magnetic field of about 1200mT. The 8-mm-thick cylindrical MAE samples with mean diameter of 18 mm were subsequently cut from the two batches for experimental characterizations.

A test rig was designed to perform experimental characterizations of aligned as well as unaligned MAEs under large amplitude oscillatory axial (LAOA) loadings. The designed test setup permitted simultaneous applications of magnetic and mechanical loadings along the axial direction. The magnetic loading was provided via an electromagnet designed with U-shaped core, as described in [21]. An electrohydraulic vibration exciter integrated into a Material Testing System was used to apply oscillatory mechanical loading (displacement-controlled mode) with selected strain magnitudes and frequencies. Figure 1 shows the schematic of the electromagnet unit, where I-core is attached to a fixed beam via a loadcell. Lower part of the electromagnet comprising the U-core was attached to the vibration exciter. Two cylindrical MAE samples were glued to stay between the upper (I-core) and lower (U-core) parts of the electromagnet during experiments, as shown in Fig. 1. The MAE samples in all the experiments were first subjected to static mechanical deformation to achieve large static pre-strain of 0.21. Dynamic loading was subsequently applied considering different strain amplitudes (ε_0), ranging from 0.025 to 0.20, at different frequencies (f) ranging from 1 to 30 Hz.

More precisely, MAE samples are initially subjected to static pre-load to achieve a pre-strain of 0.21. Harmonic motion, $\varepsilon(t) = \varepsilon_0 \sin(\omega t)$, was subsequently applied with strain amplitude, ε_0 , ranging from 0.025 to 0.20. It is noted that the reference point is the static pre-strain configuration in which strain amplitude is zero ($\varepsilon_0 = 0$). Even though the terms “compression” and “extension” generally refer to when stress response is positive ($\sigma(t) > 0$) and negative ($\sigma(t) < 0$), respectively, in this work, the authors use “compression” and “extension” cycles, correspondingly, for loading ($\varepsilon(t) > 0$) and unloading or rebound ($\varepsilon(t) < 0$). Specifically, the authors use (i) “rebound” and (ii) “extension” for unloading ($\varepsilon(t) < 0$), the second option being consistently used to make (i) the text more tangible to read and (ii) the proposed measures and interpretations be more physically applicable for other levels of pre-strains (i.e., zero pre-strain). Besides, in fact MAE samples, glued between the two poles of the electromagnet, have partially experienced extension particularly under large strain amplitudes and magnetic flux densities, even though the maximum strain amplitude (0.2) is lower than the applied pre-strain of 0.21. This is evident from negative stresses observed in hysteresis stress–strain curves (i.e., please see Figs. 2b and c, and 14 in Appendix A. Supplementary Data). This is mainly due to limited recovery during rebound/unloading of the MAE specimens considering the range of deformation and deformation-rate (1–30 Hz).

It is worth mentioning that the experiments followed ISO International Standards (ISO 4664–1) for rubbers’ dynamic properties [44]. A small-sized test apparatus was accordingly used, employing the non-resonant forced vibration method with an electrohydraulic actuator in displacement control mode. The frequency range chosen was 1 Hz (per the standard) to 30 Hz to capture steady-state stress–strain behavior of MAEs. While time-dependent and stress relaxation properties of MAEs can influence their stress–strain behavior, the primary focus of the present work is on steady-state characteristics of MAEs. However, the force level being measured by the loadcell was monitored using LABVIEW software after the pre-strain was applied. Dynamic loading was initiated once a steady-state force value was reached. The experiment design also included different levels of magnetic loading with flux density varying from zero

Fig. 2 Stress–strain characteristics of aligned MAEs subject to different amplitudes of axial strain at a frequency of 1 Hz: **a** $\varepsilon_0=0.025$, **b** $\varepsilon_0=0.10$, and **c** $\varepsilon_0=0.20$. (Magnetic flux density = 0 mT, left column; and = 750 mT, right column)



to 750 mT. The dynamic force, along with the strain (displacement) signal, was acquired in a data acquisition system for each measurement condition. It is noted that the magnetic force generated between two magnetic poles of electromagnet by turning on the magnetic field did not induce any mechanical deformation on the samples, and thus the applied pre-strain of 0.21 remained constant. However, the magnetic force generated between two poles of the electromagnet is detected by the loadcell which should be subsequently compensated. A comprehensive strategy was established in [21] to compensate for the magnetic force and thus obtain the field-dependent viscoelastic

MAE force from the total force measured by the loadcell. The experimental procedures have been described in detail in [21, 32].

3 Experimental results

Figure 2 illustrates stress–strain characteristics of the aligned MAE samples subjected to different amplitudes of dynamic axial loading, as an example, at a frequency of 1 Hz. The left and right columns of Fig. 2 illustrate the responses measured under minimum (0 mT) and maximum (750 mT) magnetic flux

density, respectively. Figure 2a illustrates the stress–strain response under strain amplitude of 0.025, which is taken as the small/medium amplitude oscillatory axial regime. In this regime, the stress–strain characteristics exhibit nearly symmetric variations and can be considered to describe nearly linear viscoelasticity behavior of MAEs. The linear response can be quantified using a single modulus (e.g., elastic modulus (E')), which can be evaluated considering the minimum ($-\varepsilon_0$) or maximum strain ($+\varepsilon_0$) during the extension and compression cycles, respectively ($E'_- = E'_+$). It can be further inferred that even though large level of pre-strain of 0.21 can contribute to asymmetry and nonlinearity of the aligned MAEs in LAOA regime, but its influence is less significant at lower level of strain amplitude even at maximum flux density of 750 mT, as shown in Fig. 2a. This is more pronounced for unaligned MAE samples, as shown in Fig. A1 in Appendix A. Supplementary Data. Increasing the strain amplitude beyond 0.025, however, causes the responses to be highly nonlinear as well as asymmetric, as shown in Fig. 2b and c for strain amplitudes of 0.10 and 0.20, respectively. These strain levels are considered to correspond to the LAOA regime. The local measures of moduli during extension ($\varepsilon(t) < 0$) and compression ($\varepsilon(t) > 0$) thus differ considerably ($E'_- \neq E'_+$). The nonlinearity and asymmetry are attributable to several factors including but not limited to pre-strain, strain amplitude, magnetic flux density and anisotropy. Increasing the strain amplitude changes the spacing between iron particles, with an increase during extension cycle and a decrease during compression, contribute to both the nonlinearity and asymmetry observed in the stress response.

Also, as Fig. 2 shows the magnetic flux density has contributed to nonlinearity and asymmetry in the stress response of the MAE to LAOA, when comparing the right column and left column of Fig. 2, corresponding to maximum and minimum applied magnetic flux density. This is in part due to the nonlinearity of the magnetization of particles, depending on particle distance, shape, and their spatial distribution, when increasing the magnetic field intensity [45, 46]. Besides, results were indicative of strong influence of anisotropy to nonlinearity and asymmetry when comparing Figs. 2 and Fig. A1 in Appendix A. Supplementary Data, respectively, for aligned and unaligned MAE samples. This is primarily

directed to the microstructure of aligned MAEs characterized by particle chains [33, 47]. For instance, comparison of Fig. 2b and A1 shows how anisotropy effect has significantly changed the curvature of stress–strain response into asymmetric shape. Apart from the asymmetry, the measured data exhibit considerable hysteresis suggesting highly nonlinear and asymmetric viscous effect, which is strongly dependent on the magnetic flux density, and also strain rate (frequency). Moreover, the measured data show nonzero mean stress corresponding to zero strain, which is due to pre-strain applied to the MAE samples.

4 New nonlinear measure

This section proposes a set of new nonlinear measures to characterize nonlinear and asymmetric behavior of MAEs subject to LAOA loading. These include differential large/zero strain moduli and large/zero strain-rate viscosity, which could also facilitate physical interpretations of the inter- and intra-cycle nonlinearities observed in asymmetric and hysteretic stress–strain responses.

4.1 Background

Considering harmonic loading, the input strain can be expressed as

$$\varepsilon(t) = \varepsilon_0 \sin(\omega t) \quad (1)$$

where ε_0 is strain amplitude, $\omega = 2\pi f$ is angular frequency and t is time. The stress response of MAEs, $\sigma(t)$, under a large amplitude harmonic strain comprises higher harmonics and can thus be approximated via Fourier series or Chebyshev polynomials. A Fourier transform (FT) analysis can be effectively used to describe contributions of higher-order harmonics to the nonlinear stress response, such that:

$$\sigma(t) = \sigma_0 + \varepsilon_0 \left[\sum_{n=1}^m E'_n(\omega, \varepsilon_0, B) \sin(n\omega t) + E''_n(\omega, \varepsilon_0, B) \cos(n\omega t) \right] \quad (2)$$

where $E'_n(\omega, \varepsilon_0, B)$ and $E''_n(\omega, \varepsilon_0, B)$ denote n th-harmonic elastic and loss moduli, respectively, as functions of ω , ε_0 , and magnetic flux density (B). σ_0 represents the nonzero mean stress, which may be attributed to static preload, and m denotes the

maximum order considered in the Fourier representation. The static component, σ_0 , is excluded in the following formulas for calculating the proposed nonlinear measures. It is because removing σ_0 doesn't impact the slope of measured stress–strain curves, and thus the elastic and loss moduli. We assumed that the effect of stress relaxation and the transient response of MAEs on σ_0 is negligible. Notably, the mean stress of MAEs generally remained constant despite variations in strain amplitude, magnetic flux density, and loading frequency. Among these factors, loading frequency had a slightly greater impact on the fluctuation of the mean stress compared to magnetic flux density and strain amplitude. The analysis of the relaxation time's effect on mean stress variation is deferred to future work.

The stress response to large amplitude oscillatory strain in shear (LAOS) comprises only the odd harmonics. Therefore, the total stress response, $\sigma(t)$, presented in Eq. (2), for MAEs subject to LAOS loading can be referred to as $\sigma_{LAOS}(t)$, and be described as the addition of elastic stress ($\sigma_{Fe}(t)$) and viscous stress ($\sigma_{Fv}(t)$) components ($\sigma_{LAOS}(t) = \sigma_{Fe}(t) + \sigma_{Fv}(t)$). The nonlinear and asymmetric stress response to LAOA strain, however, consists of odd as well as even harmonics. Under the LAOA strain, the total stress response, $\sigma(t)$, presented in Eq. (2), can be considered as a summation of elastic, viscous, and viscoelastic stress components such that $\sigma_{LAOA}(t) = \sigma_{Fe}(t) + \sigma_{Fv}(t) + \sigma_{Fve}(t)$. σ_{Fe} , σ_{Fv} , and σ_{Fve} denote Fourier elastic, viscous, and viscoelastic stresses, respectively, given by:

$$\sigma_{Fe}(t) = \varepsilon_0 \left[\sum_{n=1,3,5,\dots}^m E'_{n_{odd}}(\omega, \varepsilon_0, B) \sin(n\omega t) \right] \tag{3}$$

$$\sigma_{Fv}(t) = \varepsilon_0 \left[\sum_{n=1,3,5,\dots}^m E''_{n_{odd}}(\omega, \varepsilon_0, B) \cos(n\omega t) \right] \tag{4}$$

$$\sigma_{Fve}(t) = \varepsilon_0 \left[\sum_{n=2,4,6,\dots}^m E'_{n_{even}}(\omega, \varepsilon_0, B) \sin(n\omega t) + E''_{n_{even}}(\omega, \varepsilon_0, B) \cos(n\omega t) \right] \tag{5}$$

It is worth emphasizing that the component $\sigma_{Fve}(t)$ is zero in the shear mode considering that only odd harmonics exist in the shear stress response and the

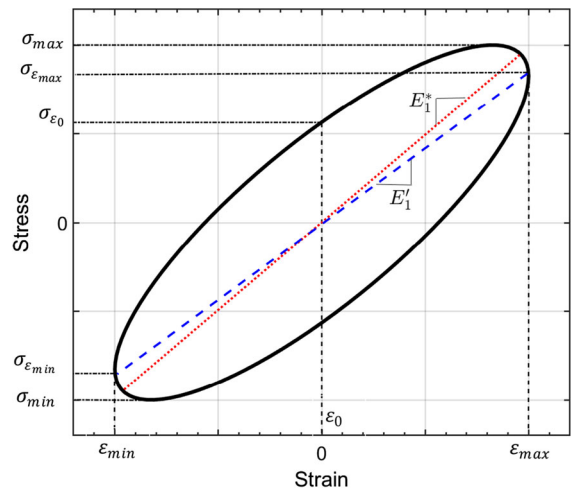


Fig. 3 Lissajous curve describing the linear and symmetric stress–strain response curve and first harmonic moduli of viscoelastic materials subject to small amplitude harmonic loading in shear or in compression/extension

shear stress–strain Lissajous curves exhibit rotational symmetry about the origin [48, 49]. Under axial loading, $\sigma_{Fve}(t)$, contributes to elastic as well as viscous nonlinearities and may be described as generalized viscoelastic moduli, $E'_{n_{even}}$ and $E''_{n_{even}}$ [30, 40]. Despite the fact that in conventional rheology, the LAOS stress response, $\sigma_{LAOS}(t)$, consisting of odd harmonics, has been referred to as viscoelastic stress response, in the present work the Fourier “viscoelastic” response, $\sigma_{Fve}(t)$, which is non-trivially separable, only belongs to the stress response to LAOA loading, $\sigma_{LAOA}(t)$.

It is worth mentioning that commercial rheometers and dynamic mechanical analyzers provide materials' characterizations on the basis of first harmonic elastic and loss moduli, E'_1 and E''_1 , which do not represent the asymmetries in responses to LAOA loading and the nonlinearities (e.g., inter-cycle strain softening and intra-cycle strain stiffening features). The first harmonic moduli possess appropriate physical interpretations only when the material response is linear and described by an elliptical stress–strain curve, as shown in Fig. 3.

The first harmonic moduli, such as complex, elastic and loss moduli, can be obtained as [44]:

$$E_1^* = \frac{\Delta\sigma}{\Delta\varepsilon} = \frac{\sigma_{\max} - \sigma_{\min}}{\varepsilon_{\max} - \varepsilon_{\min}} = E'_1 + iE''_1 \tag{6}$$

$$E'_1 = \frac{\sigma|_{\varepsilon=\varepsilon_{\max}} - \sigma|_{\varepsilon=\varepsilon_{\min}}}{\varepsilon_{\max} - \varepsilon_{\min}} = \frac{\sigma|_{\varepsilon=\varepsilon_{\max}}}{\varepsilon_{\max}} = \frac{\sigma_{\varepsilon_{\max}}}{\varepsilon_{\max}} \tag{7}$$

$$E''_1 = \frac{\sigma|_{\varepsilon=0}}{\varepsilon_{\max}} = \frac{\sigma_{\varepsilon_0}}{\varepsilon_{\max}} \tag{8}$$

where σ_{\max} , $\sigma_{\varepsilon_{\max}}$, and σ_{ε_0} are maximum stress, stress corresponding to maximum strain (ε_{\max}), and stress at zero strain, respectively. σ_{\min} refers to minimum stress and $\sigma_{\varepsilon_{\min}}$ denotes stress corresponding to minimum strain, as shown in Fig. 3. In the figure, slope of the major axis (red-dotted line) represents the complex modulus (E_1^*), while that of line joining ($\varepsilon_{\min}, \sigma_{\varepsilon_{\min}}$) and ($\varepsilon_{\max}, \sigma_{\varepsilon_{\max}}$) points defines the elastic modulus E'_1 . The ratio of loss modulus to the elastic modulus, respectively, defined in Eqs. (7) and (8), yields the loss angle ($\tan(\delta) = \frac{E''_1}{E'_1}$). The shear moduli in the linear regime can also be defined in a similar manner.

The moduli associated with higher-order harmonics (Eq. (2)) do not provide a unique interpretation of nonlinearities since they change sign depending on whether the reference input relates to sine or cosine [50]. The essential sources of nonlinearities thus cannot be described by the Fourier approximation. To address this issue, Ewoldt et al. [31] developed a framework for quantifying nonlinear viscoelasticity under LAOS loading on the basis of stress decomposition (SD) method using Chebyshev polynomial functions of first kind. Using these basis functions, the elastic and viscous contributions to the measured stress response can be given by:

$$\sigma'(x) = \gamma_0 \left[\sum_{n=\text{odd}}^m e_n(\omega, \gamma_0) T_n(x) \right] \tag{9}$$

$$\sigma''(y) = \omega\gamma_0 \left[\sum_{n=\text{odd}}^m v_n(\omega, \gamma_0) T_n(y) \right] \tag{10}$$

where $\sigma'(x)$ and $\sigma''(y)$ represent the elastic and viscous stress components. $T_n(x)$ and $T_n(y)$ are the n th-order Chebyshev polynomials of first kind, and $x = (\frac{\gamma(t)}{\gamma_0})$, and $y = (\frac{\dot{\gamma}(t)}{\omega\gamma_0})$ describe instantaneous shear strain and strain-rate, respectively. The variables x and y are selected to yield appropriate domains of orthogonality within $[-1, +1]$, and γ_0 is amplitude of harmonic shear strain $\gamma(t) = \gamma_0 \sin(\omega t)$. e_n and v_n denote the deformation-domain Chebyshev coefficients, which are independent of the arbitrary trigonometric

reference in time [50], as opposed to the time-domain Fourier coefficients.

Ewoldt et al. [31] proposed two nonlinear measures, namely, minimum and maximum strain moduli, G'_M , and G'_L , respectively, for quantifying material response under LAOS, as:

$$G'_M = \left. \frac{d\sigma}{d\gamma} \right|_{\gamma=0} = e_1 - 3e_3 + 5e_5 + \dots \tag{11}$$

$$G'_L = \left. \frac{\sigma}{\gamma} \right|_{\gamma=\gamma_0} = e_1 + e_3 + e_5 + \dots \tag{12}$$

This permitted a direct relationship between the Fourier series and Chebyshev polynomial coefficients, given by [31]:

$$e_n = G'_n (-1)^{\frac{n-1}{2}}; \quad n = 1, 3, 5, \dots \tag{13}$$

$$v_n = \frac{G''_n}{\omega}; \quad n = 1, 3, 5, \dots \tag{14}$$

Ewoldt et al. [31] thus observed only signs of the third harmonic Chebyshev coefficients for interpreting the nature of intra-cycle elastic and viscous nonlinearities, as:

$$e_3 \begin{cases} > 0 & \text{Strain-stiffening} \\ = 0 & \text{Linear viscoelastic} \\ < 0 & \text{Strain-softening} \end{cases} \quad v_3 \begin{cases} > 0 & \text{Shear-thickening} \\ = 0 & \text{Linear viscoelastic} \\ < 0 & \text{Shear-thinning} \end{cases}$$

Although shear responses are typically symmetric with respect to the direction of loading, the responses to axial loading are generally asymmetric suggesting different behavior of elastomeric materials during extension and compression. This asymmetry with respect to strain direction will result in existence of even harmonics in the Fourier spectrum. Ewoldt [30] reformulated the Fourier series including both even and odd harmonics to represent stress response to a generalized harmonic strain (e.g., $\gamma(t) = \gamma_0 \sin(\omega t)$), applicable to other deformation modes, such as extension/compression, as:

$$\sigma(t) = \gamma_0 \left[\sum_{n=0}^m G'_n \sin(n\omega t) + G''_n \cos(n\omega t) \right] \tag{15}$$

Owing to the asymmetry associated with even harmonics, the local measures of moduli differ on either side of the deformation cycle. Considering the general stress response in Eq. (15), the minimum and maximum strain moduli, G'_M , and G'_L , described in

Eqs. (11) and (12), also differ during compression and extension, which are expressed as [30]:

$$G'_{M\pm} = \frac{d\sigma}{d\gamma} \Big|_{\gamma=0; \dot{\gamma}=\pm\dot{\gamma}_0\omega} = \sum_{n:odd} nG'_n \pm \sum_{n:even} nG'_n = G'_1 \pm 2G'_2 + 3G'_3 \pm 4G'_4 + \dots \tag{16}$$

$$G'_{L\pm} = \frac{\sigma}{\gamma} \Big|_{\gamma=\pm\gamma_0} = \sum_{n:odd} G'_n(-1)^{\frac{n-1}{2}} \pm \sum_{n:even} G'_n(-1)^{\frac{n}{2}} = \pm G''_0 + G'_1 \mp G''_2 - G'_3 \pm G''_4 + \dots \tag{17}$$

In the above formulations, signs ‘+’ and ‘-’ correspond to compression and extension direction, respectively. The large and minimum rate dynamic viscosities, $\eta'_{L\pm}$ and $\eta'_{M\pm}$, can also be derived in a similar manner, as [30]:

$$\eta'_{M\pm} = \frac{d\sigma}{d\dot{\gamma}} \Big|_{\dot{\gamma}=0; \gamma=\pm\gamma_0} = \frac{1}{\omega} \sum_{n:odd} nG''_n(-1)^{\frac{n-1}{2}} \mp \frac{1}{\omega} \sum_{n:even} nG'_n(-1)^{\frac{n}{2}} = \frac{1}{\omega} (G''_1 \pm 2G'_2 - 3G''_3 \mp 4G'_4 + \dots) \tag{18}$$

$$\eta'_{L\pm} = \frac{\sigma}{\dot{\gamma}} \Big|_{\dot{\gamma}=\pm\dot{\gamma}_0\omega} = \frac{1}{\omega} \sum_{n:odd} G''_n \pm \frac{1}{\omega} \sum_{n:even} G''_n = \frac{1}{\omega} (\pm G''_0 + G'_1 \pm G''_2 + G'_3 \pm G''_4 + \dots) \tag{19}$$

In the shear mode, a direct relationship between the Chebyshev polynomial and Fourier coefficients is established, as seen in Eqs. (13) and (14). Such an explicit relationship, however, cannot be established in the presence of even harmonics in the stress response, as observed under axial deformations. This will be explained in detail in the following section. Nonetheless, a new deformation-domain orthogonal framework, other than Chebyshev polynomials, is yet to be worked out, in which a direct and explicit relationship with Fourier coefficients may be possible, when even harmonics cannot be neglected. Moreover, the large strain elastic moduli and large-rate dynamic viscosity, obtained from Eqs. (17) and (19), respectively, cannot accurately describe large nonlinearities (e.g., intra-cycle strain stiffening and strain-softening moduli) observed near extremities of the deformation cycle, as seen in Fig. 2b and c. Interestingly, these

nonlinearities and asymmetries near extremities cannot be estimated even using differential large strain moduli ($G'_{diffL\pm} = \frac{d\sigma}{d\gamma} \Big|_{\gamma=\pm\gamma_0}$), defined as the instantaneous slopes of the total stress response at the end of compression and extension cycle. It is due to the hysteretic response of MAEs, in which loading and unloading paths exhibit two different instantaneous slopes at each input strain (see Fig. 2). Similarly, the proposed minimum strain modulus $G'_{M\pm}$ and minimum rate dynamic viscosity $\eta'_{M\pm}$, obtained from Eqs. (16) and (18), cannot accurately describe the unique inter-cycle nonlinearities (e.g., strain stiffening and shear-rate thickening) at zero level of the deformation cycle, when materials are subjected to LAOA.

4.2 An alternate measure—differential large strain modulus ($E'_{DLSM\pm}$)

In this study, a new nonlinear measure, namely differential large strain modulus ($E'_{DLSM\pm}$), is proposed to quantify nonlinear and asymmetric responses of MAEs in the LAOA regime. Firstly, a Chebyshev approximation of the material response to LAOA is formulated as:

$$\sigma_T(x, y) = \sigma_0 + \varepsilon_0 \left[\sum_{n=1}^m e_n T_n(x) \right] + \omega \varepsilon_0 \left[\sum_{n=1}^m v_n T_n(y) \right] \tag{20}$$

where $\sigma_T(t)$ is stress response of the material subject to LAOA, and $x = \frac{\varepsilon(t)}{\varepsilon_0}$ and $y = \frac{\dot{\varepsilon}(t)}{\omega\varepsilon_0}$ describe the normalized strain and strain-rate, respectively, in the appropriate domains of orthogonality $[-1, +1]$ for the Chebyshev polynomials. For a harmonic strain, $\varepsilon(t) = \varepsilon_0 \sin(\omega t)$, x and y simply reduce to $\sin(\omega t)$ and $\cos(\omega t)$, respectively. In Eq. (20), σ_0 represents the mean stress associated with static pre-load ($n=0$). This static component is excluded in the subsequent formulations, since it does not affect the slope of the measured stress–strain curves, and thereby the elastic and loss moduli. The Chebyshev elastic, viscous, and viscoelastic stress components, denoted as $\sigma_{T_e}(x)$, $\sigma_{T_v}(y)$, $\sigma_{T_{ve}}(x, y)$, respectively, are subsequently defined as:

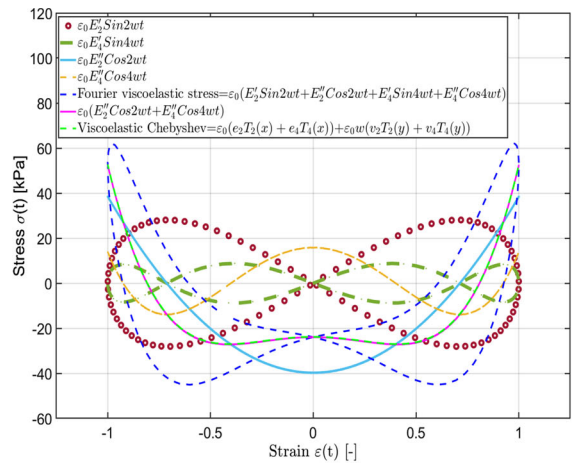
$$\sigma_{Te}(x) = \varepsilon_0 \sum_{n_{\text{odd}}} e_{n_{\text{odd}}}(\omega, \varepsilon_0, B) T_{n_{\text{odd}}}(x) \tag{21}$$

$$\sigma_{Tv}(y) = \varepsilon_0 \omega \sum_{n_{\text{odd}}} v_{n_{\text{odd}}}(\omega, \varepsilon_0, B) T_{n_{\text{odd}}}(y) \tag{22}$$

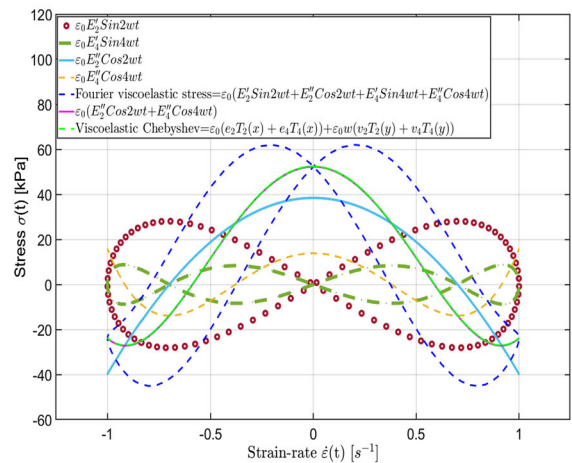
$$\begin{aligned} \sigma_{Tve}(x, y) = \varepsilon_0 \sum_{n_{\text{even}}} e_{n_{\text{even}}}(\omega, \varepsilon_0, B) T_{n_{\text{even}}}(x) \\ + \varepsilon_0 \omega \sum_{n_{\text{even}}} v_{n_{\text{even}}}(\omega, \varepsilon_0, B) T_{n_{\text{even}}}(y) \end{aligned} \tag{23}$$

Depending on whether the nature of nonlinearity of viscoelastic materials is elastic or viscous, here based on the Chebyshev stress decomposition of material response presented in Eqs. (21) to (23), we define two series of material measures namely differential zero and differential large strain modulus ($E'_{DZSM0}, E'_{DLSM\pm}$) as well as differential zero and differential large strain-rate viscosity ($\eta'_{DZSRV0}, \eta'_{DLSRV\pm}$). These materials measures, ($E'_{DZSM0}, E'_{DLSM\pm}$) and ($\eta'_{DZSRV0}, \eta'_{DLSRV\pm}$) can provide unique physical interpretations and non-linear quantifications for viscoelastic materials predominantly behave more like elastic solids and viscous liquids, respectively. The methodology does not decompose the viscoelastic stress into elastic and viscous parts, but rather simply superimpose the whole Chebyshev viscoelastic stress response to either elastic or viscous stress component. This assumption was established based on the fact that the Chebyshev viscoelastic component of the total stress response can be considered as equivalent elastic/viscous portion of the Fourier viscoelastic component in stress–strain/ stress- strain-rate Lissajous curves. This is graphically shown in Fig. 4 and will be explained in subsequent sections. The material response under LAOA may be considered nonlinearly elastic dominated (e.g., in case of MAEs) or viscous dominated (e.g., in case of MRFs). An example will be given in subsequent sections to demonstrate how the implausible (i.e., negative) values of material moduli may be used to verify the assumption of pre-dominate elastic or viscous behavior. This requires calculation of the proposed material measures at extremities of compression and extension cycles, including differential large strain moduli ($E'_{DLSM\pm}$) and differential large strain-rate viscosity ($\eta'_{DLSRV\pm}$) such that:

$$\begin{cases} E'_{DLSM\pm} > 0 & \& \eta'_{DLSM\pm} < 0 & \text{Elastic dominated} \\ E'_{DLSM\pm} < 0 & \& \eta'_{DLSM\pm} > 0 & \text{Viscous dominated} \end{cases}$$



(a)



(b)

Fig. 4 Comparison of viscoelastic response of aligned MAEs obtained from Fourier and Chebyshev approximations ($\varepsilon_0 = 0.20, B=750$ mT, and $f=1$ Hz) in terms of **a** stress vs. strain and **b** stress vs. strain-rate Lissajous curves

Therefore, for an elastic-dominated response, an equivalent nonlinear elastic Chebyshev stress, $\sigma_{Teqe}(x, y)$, is subsequently formulated as:

$$\sigma_{Teqe}(x, y) = \sigma_{Te}(x) + \sigma_{Tve}(x, y) \tag{24}$$

In this case, the elastic nonlinearities and asymmetries are entirely attributable to the viscoelastic Chebyshev coefficients. As an example, consider the expansion of $\sigma_{Teqe}(x, y)$ using Chebyshev polynomials of the first kind for $n = 2$, and $n = 4$, as:

$$\sigma_{T_{eqe}}(x, y)|_{n=2} = \varepsilon_0[e_1T_1(x)] + \varepsilon_0[e_2T_2(x) + \omega v_2T_2(y)] \tag{25}$$

$$\sigma_{T_{eqe}}(x, y)|_{n=4} = \varepsilon_0[e_1T_1(x) + e_3T_3(x)] + \varepsilon_0[e_2T_2(x) + e_4T_4(x) + \omega(v_2T_2(y) + v_4T_4(y))] \tag{26}$$

Here, as a local measure of nonlinearity, a differential large strain modulus, $E'_{DLSM\pm}$, is defined as:

$$E'_{DLSM} = \frac{d\sigma_{T_{eqe}}}{d\varepsilon} \Big|_{\varepsilon=\varepsilon_0} = \frac{d\sigma_{T_{eqe}}}{\varepsilon_0 dx} \Big|_{x=1} \tag{27}$$

Since the even harmonics exhibit asymmetry, the proposed local measures in Eq. (27) can yield different modulus during extension and compression, and may be expressed as:

$$E'_{DLSM\pm} = \frac{d\sigma_{T_{eqe}}}{d\varepsilon} \Big|_{\varepsilon=\pm\varepsilon_0} = \frac{d\sigma_{T_{eqe}}}{\varepsilon_0 dx} \Big|_{x=\pm 1} \tag{28}$$

For instance, the proposed local measures, $E'_{DLSM\pm}$, during compression (+) and extension (-) for $n=2$ and 4, can be computed considering the Chebyshev polynomials of the first kind as:

$$E'_{DLSM\pm} = \frac{d\sigma_{T_{eqe}}}{\varepsilon_0 dx} \Big|_{x=\pm 1; n=2} = [e_1] \pm 4[e_2 \mp \omega v_2] \tag{29}$$

$$E'_{DLSM\pm} = \frac{d\sigma_{T_{eqe}}}{\varepsilon_0 dx} \Big|_{x=\pm 1; n=4} = [e_1 + 9e_3] \pm 4[(e_2 + 4e_4) \mp \omega(v_2 - 4v_4)] \tag{30}$$

It should be noted that unlike the slope of the loading/unloading paths of total stress, $E'_{DLSM\pm}$ is deliberately chosen as the slope of the equivalent nonlinear elastic stress corresponding to maximum and minimum strains observed during compression and extension cycles, respectively, such that both converge to linear strain-independent elastic modulus ($E'_1(\omega)$) under relatively small strain inputs. Likewise, this choice provides a unique value of instantaneous slope (local differential measure) for each level of applied strain, thereby realizing unique interpretation of intra-cycle nonlinearities, such as strain stiffening effect in compression and extension segments of the stress response.

A differential zero strain modulus (E'_{DZSM_0}) is further defined to quantify inter-cycle nonlinearities

(e.g., strain amplitude stiffening/softening) of the material, as:

$$E'_{DZSM_0} = \frac{d\sigma_{T_{eqe}}}{\varepsilon_0 dx} \Big|_{x=0; n=2} = e_1 \tag{31}$$

$$E'_{DZSM_0} = \frac{d\sigma_{T_{eqe}}}{\varepsilon_0 dx} \Big|_{x=0; n=4} = e_1 - 3e_3 \tag{32}$$

Relative magnitudes of E'_{DZSM_0} and $E'_{DLSM\pm}$ permit unique interpretations of intra-cycle nonlinearities, as discussed in the following sections.

It is also worth emphasizing that increasing the order of the Chebyshev polynomial beyond four ($n > 4$) didn't notably enhance the stress prediction. Conversely, reducing the order below four ($n < 4$) quite significantly compromised stress approximation accuracy. Consequently, in this work the nonlinear measures were determined based on the fourth-order Chebyshev polynomial ($n=4$). To substantiate our choice, we include Fig. A2 in Appendix A. Supplementary Data. This figure compares the second-, fourth-, sixth-, and eighth-order Chebyshev stress approximations, as an example for the measured stress-strain characteristics of an aligned MAE subjected to LAOA loading, both qualitatively and quantitatively (i.e., R^2 or the coefficient of determination).

4.3 Equivalent set of Fourier coefficients for the proposed measures

In the previous section, it is shown that Chebyshev polynomials approximation of the stress response of MAEs subject to LAOA permits determination of equivalent nonlinear elastic stress and thus quantify nonlinear characteristics in terms of the local moduli. In this section, we seek a set of equivalent Fourier coefficients for the same nonlinear analysis. This can yield two important advantages. Firstly, Fourier series analysis has been mostly provided in the software of dynamic mechanical characterization devices (e.g., dynamic mechanical analyzers). Secondly, given the same n th partial sum, the rate of convergence in Fourier series is much faster than that of the Chebyshev polynomial, when approximating a non-polynomial function (e.g., highly nonlinear stress response) [51]. The Fourier representations of the viscoelastic materials response to a LAOA loading, $\sigma_F(t)$, is thus

used to obtain the proposed differential moduli, E'_{DZSM_0} and $E'_{DLSM_{\pm}}$, as:

$$\sigma_F(t) = \varepsilon_0 \left[\sum_{n=1}^m E'_n(\omega, \varepsilon_0, B) \sin(n\omega t) + E''_n(\omega, \varepsilon_0, B) \cos(n\omega t) \right] \tag{33}$$

Here, the Fourier elastic, viscous, and viscoelastic stress components, $\sigma_{Fe}(t)$, $\sigma_{Fv}(t)$, $\sigma_{Fve}(t)$, respectively, are defined as:

$$\sigma_{Fe}(t) = \varepsilon_0 \left[\sum_{n=odd}^m E'_n(\omega, \varepsilon_0, B) \sin(n\omega) \right] \tag{34}$$

$$\sigma_{Fv}(t) = \varepsilon_0 \left[\sum_{n=odd}^m E''_n(\omega, \varepsilon_0, B) \cos(n\omega) \right] \tag{35}$$

$$\sigma_{Fve}(t) = \varepsilon_0 \left[\sum_{n=even}^m E'_n(\omega, \varepsilon_0, B) \sin(n\omega t) + E''_n(\omega, \varepsilon_0, B) \cos(n\omega t) \right] \tag{36}$$

In case of a predominately elastic behavior, an equivalent nonlinear elastic Fourier stress, $\sigma_{F_{eqe}}$, is obtained from:

$$\sigma_{F_{eqe}}(t) = \sigma_{Fe}(t) + \sigma_{Fve}(t) \tag{37}$$

Equation (37), as an example, may be simplified considering $n=2$ and $n=4$, as:

$$\sigma_{F_{eqe}}(t; x, y) \Big|_{n=2} = \varepsilon_0 [E'_1 \sin(\omega t)] + \varepsilon_0 [E'_2 \sin(2\omega t) + E''_2 \cos(2\omega t)] \tag{38}$$

$$\sigma_{F_{eqe}}(x, y) \Big|_{n=4} = \varepsilon_0 [E'_1 \sin(\omega t) + E'_3 \sin(3\omega t) + \varepsilon_0 [E'_2 \sin(2\omega t) + E''_2 \cos(2\omega t) + E'_4 \sin(4\omega t) + E''_4 \cos(4\omega t)] \tag{39}$$

The differential zero strain modulus (E'_{DZSM_0}) can be directly and explicitly obtained from the equivalent nonlinear elastic Fourier stress, $\sigma_{F_{eqe}}$, as:

$$E'_{DZSM_0} = \frac{d\sigma_{F_{eqe}}}{\varepsilon_0 dx} \Big|_{x=0; n=2} = E'_1 + 2E'_2 \tag{40}$$

$$E'_{DZSM_0} = \frac{d\sigma_{F_{eqe}}}{\varepsilon_0 dx} \Big|_{x=0; n=4} = E'_1 + 3E'_3 + 2E'_2 + 4E'_4 \tag{41}$$

The $E'_{DLSM_{\pm}}$ moduli can also be subsequently obtained as:

$$E'_{DLSM_{\pm}} = \frac{d\sigma_{F_{eqe}}}{d\varepsilon} \Big|_{\varepsilon \approx \pm \varepsilon_0; n=2 \& 4} = \frac{d\sigma_{F_{eqe}}}{\varepsilon_0 dx} \Big|_{x \approx \pm 1; n=2 \& 4} \tag{42}$$

It should be noted that the proposed local measures, $E'_{DLSM_{\pm}}$, in Eqs. (29) and (30) are derived from the Chebyshev polynomials of first kind considering $x = \pm 1$. Unlike the Chebyshev polynomials representation, the $E'_{DLSM_{\pm}}$ in case of Fourier representation must be obtained at $x \neq \pm 1$ in order to eliminate potential singularities. This is due to the presence of even *sine* terms (e.g., $\sin(2\omega t) = 2\sin(\omega t)\cos(\omega t) = 2xy$), given the facts that $x = \left(\frac{\gamma(t)}{\gamma_0}\right) = \sin(\omega t)$, and $y = \left(\frac{\dot{\gamma}(t)}{\omega\gamma_0}\right) = \cos(\omega t)$, and $y = \sqrt{1 - x^2}$. The Chebyshev polynomial approximations with even terms, on the other hand, contain even powers (e.g., y^2, y^4, \dots). A direct explicit relationship between Chebyshev polynomials and Fourier series coefficients has been lacking primarily due to even *sine* terms. The $E'_{DLSM_{\pm}}$, obtained from Eq. (42), is thus highly sensitive to the value x near the extremities ($x \approx \pm 1$). A suitable value for x may permit derivation of an explicit, although not a general, relationship between the Fourier coefficients and Chebyshev polynomials, by equating Eqs. (28) and (42). A relation between the Chebyshev and Fourier coefficients is presented in Table B.1 in Appendix B. Supplementary Data, considering $x = \pm 0.99$, as an example.

It should be noted that finding a direct and explicit relationship between the Fourier coefficients and Chebyshev polynomials for the entire domain of orthogonality ($[-1, 1]$) is impossible, when even harmonic cannot be neglected. Since a Chebyshev polynomial expansion is merely a Fourier cosine series in disguise [52], following a change of variable ($z = \cos\theta$) under the mapping of ($T_n(\cos\theta) = \cos n\theta$). In other words, the coefficients of $f(z)$ as a Chebyshev series are identical to the Fourier cosine coefficients, $f(\cos\theta)$. This may also be observed from Eq. (14). In order to obtain the nonlinear equivalent Chebyshev

Table 1 Relationships between coefficients of Fourier series and Chebyshev polynomials for viscoelastic materials assuming elastic/viscous dominated behavior under LAOA loading ($n = 4$)

Chebyshev	e_1	e_2	e_3	e_4	v_1	v_2	v_3	v_4
	E'_1	$\omega v_2 - E''_2$	$-E_3'$	$E''_4 - \omega v_4$	E''_1/ω	$(e_2 + E''_2)/\omega$	E''_3/ω	$(E''_4 - e_4)/\omega$
Fourier	E_1'	E_2'	E_3'	E_4'	E''_1	E''_2	E''_3	E''_4
	e_1	—	$-e_3$	—	ωv_1	$\omega v_2 - e_2$	ωv_3	$\omega v_4 + e_4$

stress, $\sigma_{T_{eqe}}$, presented in Eq. (26), from the Fourier series, the even *sine* terms can be ignored. Since the even *cosine* terms of the Fourier expansion of the stress response are exactly the same as the Chebyshev viscoelastic stress component. This is also shown graphically in Figs. 4(a) and 4(b), through comparison of the Chebyshev viscoelastic stress component with Fourier viscoelastic stress, and its components in the stress–strain and stress- strain-rate Lissajous plots. It can be observed that the Chebyshev viscoelastic component of the stress response can be considered as equivalent elastic/viscous portion of the Fourier viscoelastic component in stress–strain and stress-strain-rate Lissajous curves. Considering $n = 4$, as an example, an implicit but unique relationship, can thus be derived between the Fourier coefficients and Chebyshev polynomials, by equating the Fourier and Chebyshev viscoelastic components, and using the transformation of $(T_n(\cos\theta) = \cos n\theta)$. This relationship is shown in Table 1 considering $n = 4$. Although the coefficients within this relationship are not explicitly related, the resulting equity is of great importance due to the two advantages mentioned in the beginning of Sect. 4.3. The equivalent elastic/viscous Chebyshev stress ($\sigma_{T_{eqe}}/\sigma_{T_{eqv}}$) can, hence, be obtained by excluding the *sine* terms in the equivalent elastic/viscous Fourier stress ($\sigma_{F_{eqe}}/\sigma_{F_{eqv}}$), it can be referred to as ($\sigma_{F'_{eqe}}/\sigma_{F'_{eqv}}$). Subsequently, the exact set of nonlinear measures, $E'_{DLSM\pm}$, and E'_{DZSM_0} , respectively, presented in Eqs. (30) and (32), can be more quickly obtained from the corresponding Fourier coefficients by taking derivative of $\sigma_{F'_{eqe}}/\sigma_{F'_{eqv}}$ with respect to the imposed strain. Considering $n=2$ and 4, these moduli are obtained as:

$$E'_{DLSM\pm} = \frac{d\sigma_{F'_{eqe}}}{\varepsilon_0 dx} \Big|_{x=\pm 1;n=2} = E'_1 \mp 4E''_2 \tag{43}$$

$$E'_{DLSM\pm} = \frac{d\sigma_{F'_{eqe}}}{\varepsilon_0 dx} \Big|_{x=0;n=4} = E'_1 - 9E'_3 \mp 4E''_2 \pm 16E''_4 \tag{44}$$

$$E'_{DZSM_0} = \frac{d\sigma_{F'_{eqe}}}{\varepsilon_0 dx} \Big|_{x=0;n=4} = E'_1 + 3E'_3 \tag{45}$$

where $\sigma_{F'_{eqe}}$ is exactly equivalent to the equivalent nonlinear elastic Chebyshev stress, $\sigma_{T_{eqe}}$, presented in Eq. (26).

Figure 4 further highlights the important fact that unlike the Chebyshev viscoelastic stress, the Fourier viscoelastic stress cannot be superimposed to Fourier elastic/viscous stress to yield equivalent elastic/viscous stress. It is because the Fourier viscoelastic stress provides two values for each instant of input strain, thereby impeding uniquely quantifying material non-linearity under LAOA loading.

Apart from $E'_{DLSM\pm}$, a differential large strain-rate viscosity ($\eta'_{DLSRV\pm}$) can also be defined for materials showing predominately elastic behavior. Assuming that the viscous component, described in Eq. (22), is nearly symmetric, and thereby negligible contribution due to even harmonics in the viscoelastic stress component. The $\eta'_{DLSRV\pm}$ measures obtained from the Chebyshev and Fourier viscous stress can be expressed as:

$$\eta'_{DLSRV\pm} = \frac{d\sigma_{T_v}}{d\dot{\varepsilon}} \Big|_{\dot{\varepsilon}=\pm \varepsilon_0 \omega} = \frac{d\sigma_{T_v}}{\varepsilon_0 \omega dy} \Big|_{y=\pm 1} \tag{46}$$

$$\eta'_{DLSRV\pm} = \frac{d\sigma_{F_v}}{d\dot{\varepsilon}} \Big|_{\dot{\varepsilon}=\pm \varepsilon_0 \omega} = \frac{d\sigma_{F_v}}{\varepsilon_0 \omega dy} \Big|_{y=\pm 1} \tag{47}$$

Considering $n = 4$ in the Chebyshev and Fourier viscous stress approximations, as an example, the $\eta'_{DLSRV\pm}$ are obtained as:

$$\eta'_{DLSRV_{\pm}} = \frac{d\sigma_{T_v}}{\varepsilon_0 \omega dy} \Big|_{y=\pm 1; n=4} = v_1 + 9v_3 \quad (48)$$

$$\eta'_{DLSRV_{\pm}} = \frac{d\sigma_{F_v}}{\varepsilon_0 \omega dy} \Big|_{y=\pm 1; n=4} = \frac{1}{\omega} (E''_1 + 9E''_3) \quad (49)$$

The inter/intra-cycle viscous nonlinearities (e.g., shear thinning) in viscoelastic materials showing elastic-dominated behavior can be quantified considering the differential zero strain-rate viscosity (η'_{DZSRV_0}). This measure is also defined from the Chebyshev and Fourier viscous stress responses, as:

$$\eta'_{DZSRV_0} = \frac{d\sigma_{T_v}}{d\dot{\varepsilon}} \Big|_{\dot{\varepsilon}=0} = \frac{d\sigma_{T_v}}{\varepsilon_0 \omega dy} \Big|_{y=0} \quad (50)$$

$$\eta'_{DZSRV_0} = \frac{d\sigma_{F_v}}{d\dot{\varepsilon}} \Big|_{\dot{\varepsilon}=0} = \frac{d\sigma_{F_v}}{\varepsilon_0 \omega dy} \Big|_{y=0} \quad (51)$$

Considering $n = 4$, as an example, η'_{DLSRV_0} derived from σ_{T_v} and σ_{F_v} are given by:

$$\eta'_{DZSRV_0} = \frac{d\sigma_{T_v}}{\varepsilon_0 \omega dy} \Big|_{y=0; n=4} = v_1 - 3v_3 \quad (52)$$

$$\eta'_{DZSRV_0} = \frac{d\sigma_{F_v}}{\varepsilon_0 \omega dy} \Big|_{y=0; n=4} = \frac{1}{\omega} (E''_1 - 3E''_3) \quad (53)$$

The proposed differential moduli measures, presented in Sects. 4.2 to 4.3, can also be obtained for materials showing viscous-dominated behavior in a similar manner, as presented in Appendix B. Supplementary Data. In the small strain limits (i.e., $e_2 \& e_3 \ll e_1$), the proposed nonlinear measures for elastic nonlinearities ($E'_{DLSM_{\pm}}$) converge to the linear elastic modulus ($E'_{DLSM_{\pm}} = E'_1 = e_1$), as can be seen from Eqs. (29)–(30) and Eqs. (38)–(42). The $\eta'_{DLSRV_{\pm}}$ can also be related to the constant loss modulus in the linear regime, i.e., $\eta'_{DLSRV_{\pm}} = v_1 = \frac{E''_1}{\omega}$.

The relative magnitudes of $E'_{DLSM_{\pm}}$ and $\eta'_{DLSRV_{\pm}}$ obtained for compression and extension can also facilitate qualitative interpretations of the nature of elastic and viscous intra-cycle nonlinearities for each loading path, thereby observing which loading mechanism offers more stiffening/dampening behavior. These are referred to as strain asymmetric stiffening/dampening, which are briefly described in Fig. 5a. For example, if we observe that $\eta'_{DLSRV_{+}} > \eta'_{DLSRV_{-}}$ for an MAE subjected to a LAOA loading, the MAE

shows strain asymmetric dampening effect. It simply indicates that the MAE sample has unevenly dissipated energy as strain increases. Specifically, it has dissipated more energy during the compression cycle than during the extension cycle, resulting in non-symmetric energy dissipation. It is expected that the shape of stress–strain curve response to be asymmetric with respect to origin.

Likewise, the proposed measures, E'_{DZSM_0} , and η'_{DZSRV_0} , together with $E'_{DLSM_{\pm}}$ and $\eta'_{DLSRV_{\pm}}$ can also facilitate interpretations of other intra-cycle nonlinearities, such as compression/extension stiffening/softening, and compression-/extension-rate thickening/thinning, as shown in Fig. 5b. For instance, if for a viscoelastic material subject to a LAOA loading, $E'_{DLSM_{+}} > E'_{DLSM_0}$ then the material shows intra-cycle stiffening effect when it deforms during compression path (see point A_1 in Fig. 5b). Point A_2 refers to a case that the material shows linear viscoelasticity as $\eta'_{DLSRV_{+}} = \eta'_{DZSRV_0}$. Point A_3 is located under the line corresponds to the linear viscoelasticity regime, thereby referring to a case that material shows extension-rate thinning behavior ($\eta'_{DLSRV_{-}} < \eta'_{DZSRV_0}$), simply meaning that as the rate of oscillation in extension path increases the viscosity of the material declines.

4.4 Dimensionless index of asymmetry

The proposed nonlinear elastic and viscous measures can also be effectively used to define dimensionless indices for analyzing cyclic asymmetry under LAOA loading and facilitating better interpretations and understanding of intra-cycle stiffening and dampening during compression and extension. These dimensionless indices can also permit identifications of inter-cycle nonlinearities under different mechanical and magnetic field stimuli, which are briefly described below.

4.4.1 Intra-cycle nonlinearities

The intra-cycle asymmetry in the response can be expressed by the asymmetry ratios in terms of elastic ($AR_{+/-}^e$) and viscous ($AR_{+/-}^v$) characteristics, as:

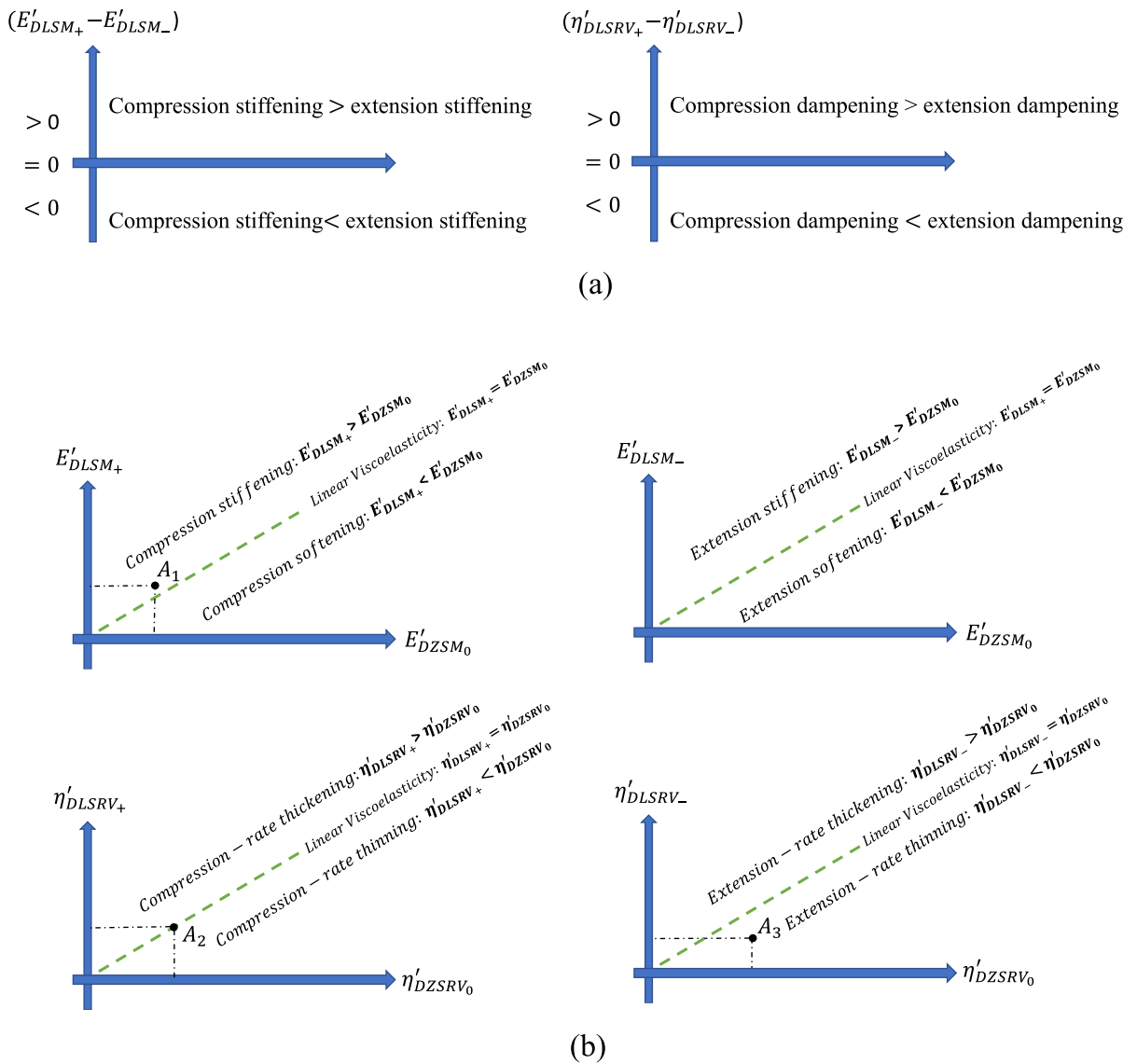


Fig. 5 Domains of inter/intra-cycle elastic and viscous nonlinearities from the proposed set of new nonlinear measures: **a** only large strain moduli, and **b** zero and large strain/strain rate moduli

$$AR_{+/-}^e = \frac{E'_{DLSM+}}{E'_{DLSM-}} \tag{54}$$

$$AR_{+/-}^v = \frac{\eta'_{DLSRV+}}{\eta'_{DLSRV-}} \tag{55}$$

A unity value of AR refers to linear and symmetric viscoelastic response. $AR_{+/-}^e > 1$ and $AR_{+/-}^v > 1$ represent higher stiffening and dampening, respectively, in compression than in extension. Similarly, an

opposite behavior is observed for $AR_{+/-}^e < 1$ and $AR_{+/-}^v < 1$.

4.4.2 Inter-cycle nonlinearities

The response behavior of a magneto-active material is strongly dependent on the magnitude and rate of applied mechanical load (ϵ_0, ω), apart from the magnetic flux density (B). The inter-cycle nonlinearities, such as strain amplitude softening, strain amplitude stiffening, strain-rate stiffening and magnetic

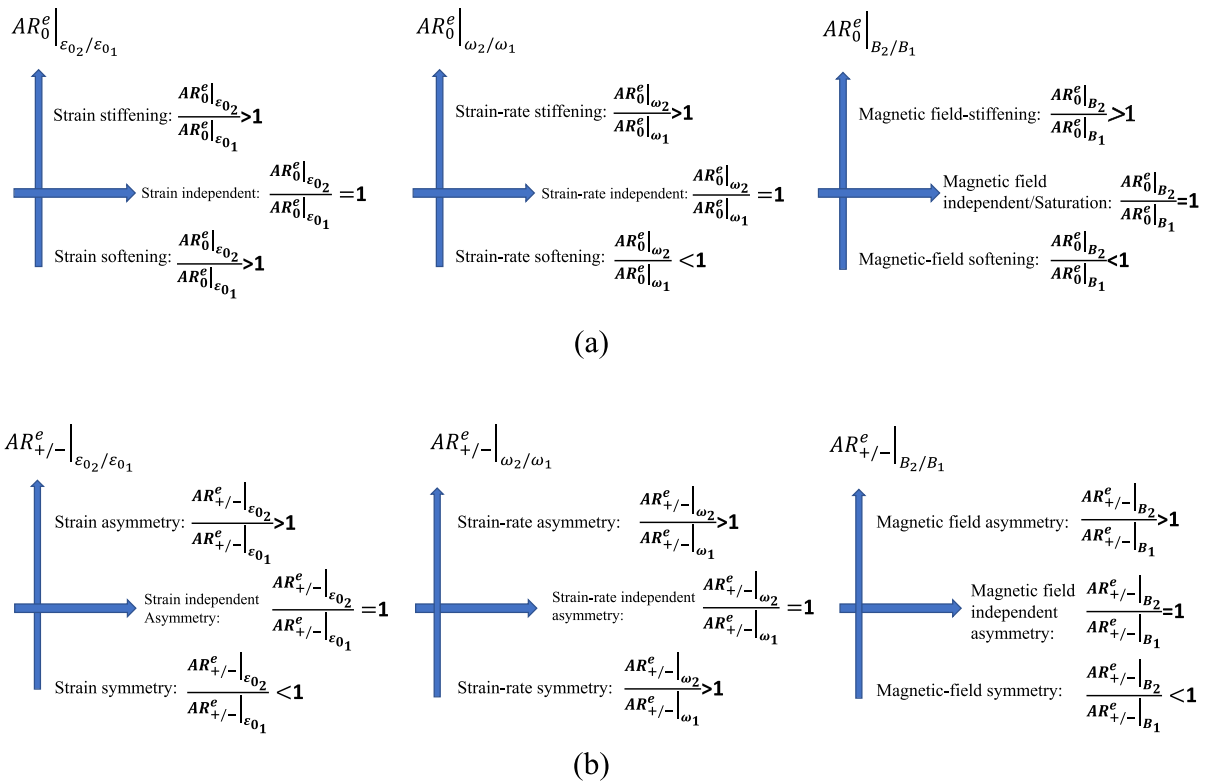


Fig. 6 Relative values of proposed dimensionless indices of asymmetry corresponding to zero and large strains illustrating the domains of inter-cycle nonlinearities: **a** symmetric and **b** asymmetric

field-stiffening have been observed for MAEs in many studies (e.g., [32, 53, 54]). The proposed nonlinear measures can provide essential guidance concerning these inter-cycle nonlinearities. For instance, the inter-cycle strain softening can be inferred as a decrease in stiffness with increase in strain amplitude. Therefore, the proposed nonlinear measures at zero strain and zero strain rate, E'_{DZSM_0} and η'_{DZSRV_0} , can be used to interpret the effects of magneto-mechanical loading conditions on MAE's behavior between two cycles of LAOA loading. Likewise, inter-cycle strain stiffening can be inferred as the increase in local slope at compression or extension extremities with increase in strain amplitude. The inter-cycle elastic and viscous asymmetry ratios, AR_0^e and AR_0^v , corresponding to two different loading conditions (ϵ_0, ω, B) can be evaluated as:

$$AR_0^e = \frac{E'_{DZSM_0} |_{\epsilon_{02}; \omega_2; B_2}}{E'_{DZSM_0} |_{\epsilon_{01}; \omega_1; B_1}} \tag{56}$$

$$AR_0^v = \frac{\eta'_{DZSRV_0} |_{\epsilon_{02}; \omega_2; B_2}}{\eta'_{DZSRV_0} |_{\epsilon_{01}; \omega_1; B_1}} \tag{57}$$

Thus, by considering two different values of strain amplitude ($\epsilon_{02} > \epsilon_{01}$), strain-rate ($\omega_2 > \omega_1$), and magnetic flux density ($B_2 > B_1$) inputs, different interpretations for inter-cycle nonlinearities can be deduced as shown in Fig. 6a.

The nonlinear measures described in Eqs. (16) thru (18) provide non-unique values for material responses to a LAOA input corresponding to zero strain/strain-rate [30]. The above-stated interpretations of inter-cycle nonlinearities can be uniquely realized via the material measures proposed in the present work, defined in Eqs. (31) and (32), and (52) and (53). Apart from inter-cycle symmetric nonlinearities shown in Fig. 6a, the inter-cycle asymmetric nonlinearities can also be interpreted by comparing the asymmetry ratio obtained for two sets of magneto-mechanical loading conditions, as shown in Fig. 6b. For instance, when strain amplitude increases from ϵ_{01} to ϵ_{02} , then

Table 2 Comparisons of the proposed differential large/zero strain moduli ($E'_{DLSM_{\pm}}$, and E'_{DZSM_0}) with ($G'_{L_{\pm}}$, and $G'_{M_{\pm}}$) obtained for the unaligned MAEs subject to LAOA loading ($\epsilon_0=0.1$ and 0.2 , $f=1$ Hz, and $B=750$ mT)

$E'_{DLSM_{\pm}}$ (kPa)	$\epsilon_0=0.1$			$\epsilon_0=0.2$		
	Extension $E'_{DLSM_{-}}$	$AR^e_{+/-}$	Compression $E'_{DLSM_{+}}$	Extension $E'_{DLSM_{-}}$	$AR^e_{+/-}$	Compression $E'_{DLSM_{+}}$
	1231	2.8	3460	123	40	4891
E'_{DZSM_0} (kPa)	496			52		
$G'_{L_{\pm}}$ (kPa) [30]	$\epsilon_0=0.1$			$\epsilon_0=0.2$		
	Extension $G'_{L_{-}}$	$AR^e_{+/-}$	Compression $G'_{L_{+}}$	Extension $G'_{L_{-}}$	$AR^e_{+/-}$	Compression $G'_{L_{+}}$
	942	1.35	1268	561	2	1163
$G'_{M_{\pm}}$ (kPa) [30]	$\epsilon_0=0.1$			$\epsilon_0=0.2$		
	Extension $G'_{M_{-}}$	$AR^e_{+/-}$	Compression $G'_{M_{+}}$	Extension $G'_{M_{-}}$	$AR^e_{+/-}$	Compression $G'_{M_{+}}$
	295	2.4	698	- 205	- 1.5	310

Table 3 Comparisons of the proposed differential large/zero strain-rate viscosity ($\eta'_{DLSRV_{\pm}}$, and η'_{DZSRV_0}) with ($\eta'_{L_{\pm}}$, and $\eta'_{M_{+}}$) obtained for the unaligned MAEs subject to LAOA loading ($\epsilon_0=0.1$ and 0.2 , $f=1$ Hz, and $B=750$ mT)

$\eta'_{DLSRV_{\pm}}$ (kPa.s)	$\epsilon_0=0.1$			$\epsilon_0=0.2$		
	Extension $\eta'_{DLSRV_{-}}$	$AR^v_{+/-}$	Compression $\eta'_{DLSRV_{+}}$	Extension $\eta'_{DLSRV_{-}}$	$AR^v_{+/-}$	Compression $\eta'_{DLSRV_{+}}$
	29.49	1	29.49	≈ 0	1	≈ 0
η'_{DZSRV_0} (kPa.s)	145.93			140.04		
$\eta'_{L_{\pm}}$ (kPa.s) [30]	$\epsilon_0=0.1$			$\epsilon_0=0.2$		
	Extension $\eta'_{L_{-}}$	$AR^v_{+/-}$	Compression $\eta'_{L_{+}}$	Extension $\eta'_{L_{-}}$	$AR^v_{+/-}$	Compression $\eta'_{L_{+}}$
	121.37	0.77	92.87	93.84	0.62	58.37
$\eta'_{M_{\pm}}$ (kPa.s) [30]	$\epsilon_0=0.1$			$\epsilon_0=0.2$		
	Extension $\eta'_{M_{-}}$	$AR^v_{+/-}$	Compression $\eta'_{M_{+}}$	Extension $\eta'_{M_{-}}$	$AR^v_{+/-}$	Compression $\eta'_{M_{+}}$
	91.40	2.19	200.45	40.49	5.92	239.57

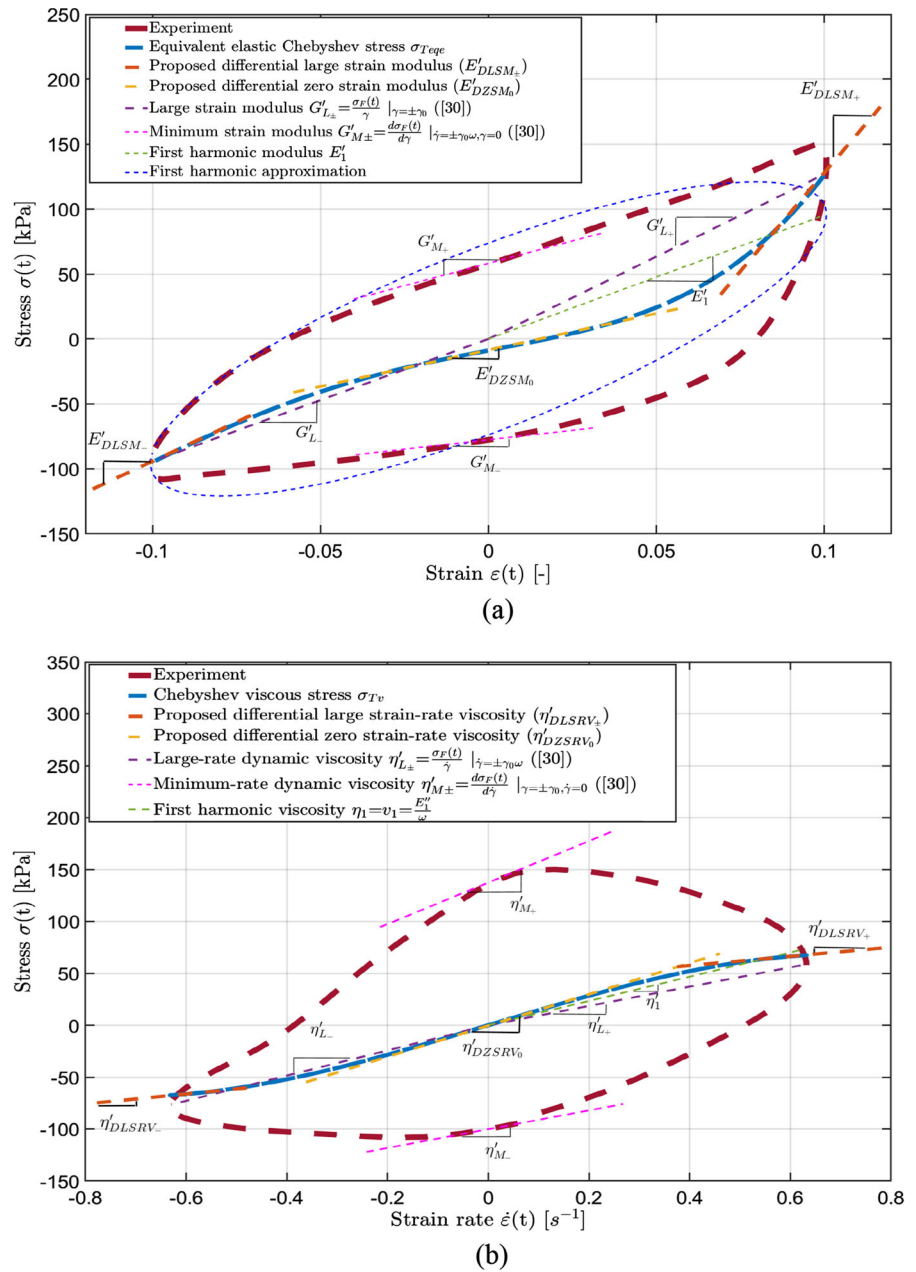
$AR^e_{+/-} \Big|_{\epsilon_0_2/\epsilon_0_1}$ may become greater than 1, suggesting strain asymmetry, i.e., increasing asymmetry in material response with increasing strain amplitude. Similarly, an opposite behavior is identified strain symmetry (asymmetry weakening effect) for $AR^e_{+/-} \Big|_{\epsilon_0_2/\epsilon_0_1} < 1$. The proposed set of nonlinear measures presented in this section have been determined for both the unaligned and aligned MAE samples under different ranges of magneto-mechanical loading conditions and summarized in Table C.1 through C.6, in Appendix C. Supplementary Data. The coefficients of the Fourier series and Chebyshev polynomials were identified through minimization of square of error between the experimental total stress and those predicted by the Fourier series and Chebyshev polynomials. The error minimization was

performed using the nonlinear gradient-based optimization algorithm, namely Sequential Quadratic Programming, in MATLAB. The Fourier series converged faster than the Chebyshev polynomial in approximating the total stress response, particularly at higher strain amplitudes.

4.5 Schematic representation of the proposed material measures.

This section presents a schematic representation of the proposed material measures, offering a visual insight into the key concepts described in previous subsections. Within this representation, the effectiveness of the proposed framework for quantifying nonlinear and asymmetric characteristics of MAEs subject to LAOA is also assessed by comparing the differential large/zero strain moduli ($E'_{DLSM_{\pm}}/E'_{DZSM_0}$) and differential

Fig. 7 Comparisons of proposed differential large/zero strain ($E'_{DLSM\pm}$ and E'_{DZSM0}) and large/zero strain-rate ($\eta'_{DLSRV\pm}$ and η'_{DZSRV0}) moduli determined for the unaligned MAE samples with the nonlinear measures ($G'_{M\pm}$, $G'_{L\pm}$, $\eta'_{M\pm}$, and $\eta'_{L\pm}$) reported in [30], obtained from stress–strain **a** and stress–strain-rate **b** responses ($\varepsilon_0=0.1$, $f=1$ Hz, and $B=750$ mT)

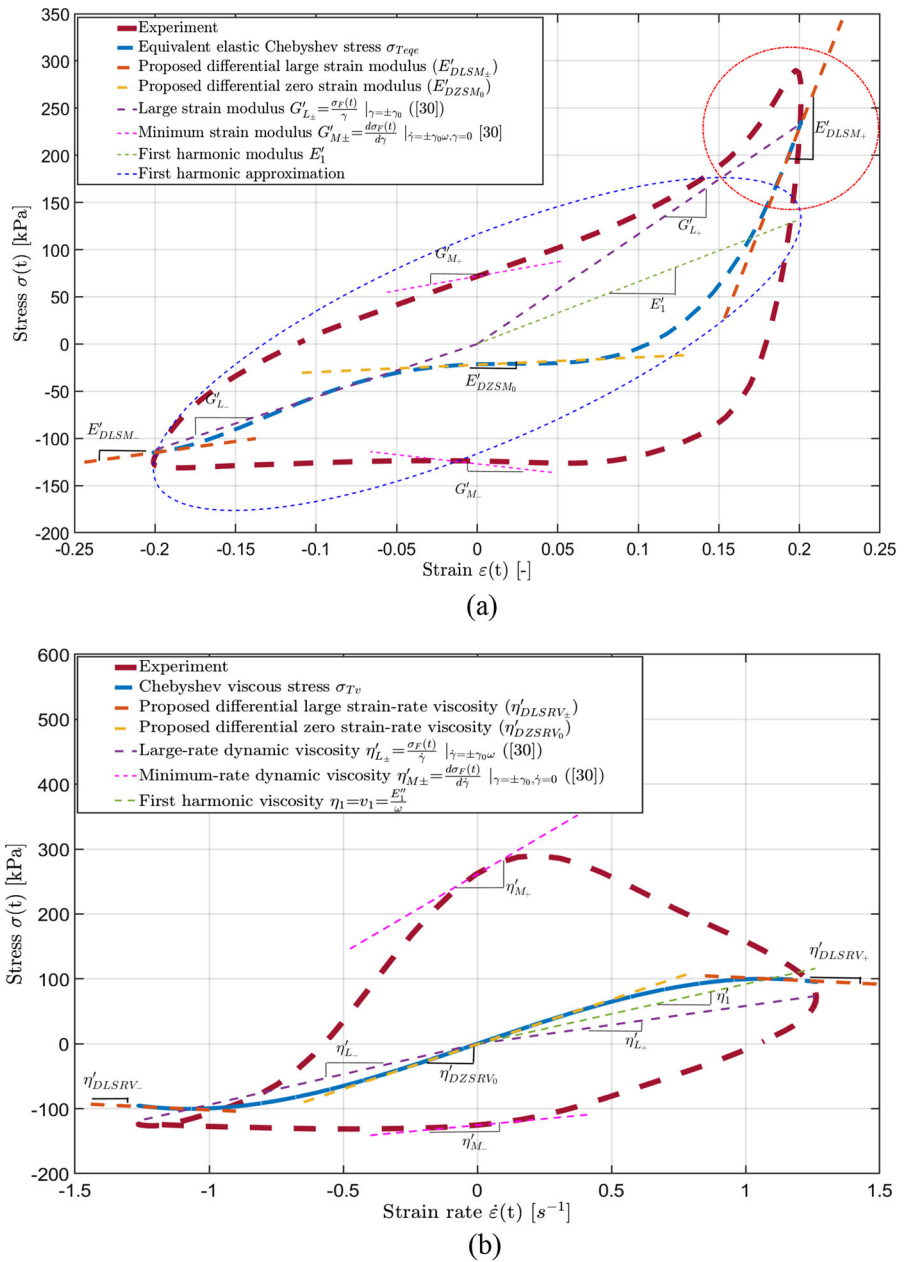


large/zero strain-rate viscosity ($\eta'_{DLSRV\pm}/\eta'_{DZSRV0}$) with the reported measures in [30]. These include the large/minimum strain moduli ($G'_{L\pm}/G'_{M\pm}$), and large/minimum rate dynamic viscosity ($\eta'_{L\pm}/\eta'_{M\pm}$). The comparisons are presented in Table 2 and 3, as well as Figs. 7 and 8, considering $f = 1$ Hz and $B = 750$ mT, as an example. The results are presented for an unaligned MAE sample subject to two strain amplitudes ($\varepsilon_0=0.1$

and 0.2). Figures 7 and 8 also show the first harmonic moduli.

The comparisons suggest that the measures $G'_{L\pm}$ underestimate local nonlinearities near the maximum and minimum strains when compared with the proposed nonlinear measures. Moreover, the proposed asymmetry ratio indices permit quantitative and qualitative identification of nonlinearities, as seen in Table 2 and Lissajous curves presented in Figs. 7 and

Fig. 8 Comparisons of proposed differential large/zero strain ($E'_{DLSM_{\pm}}$ and E'_{DZSM_0}) and large/zero strain-rate ($\eta'_{DLSRV_{\pm}}$ and η'_{DZSRV_0}) moduli determined for the unaligned MAE samples with the nonlinear measures ($G'_{M_{\pm}}$, $G'_{L_{\pm}}$, $\eta'_{M_{\pm}}$, and $\eta'_{L_{\pm}}$) reported in [30], obtained from stress–strain **a** and stress–strain-rate **b** responses ($\epsilon_0=0.2$, $f=1$ Hz, and $B=750$ mT)



8. For instance, $E'_{DLSM_{+}}$ increases from 3460 to 4891 kPa when the strain amplitude increases from 0.1 to 0.2. This local inter-cycle strain amplitude stiffening has also been observed for aligned MAEs as shown in Fig. 2, when the strain amplitude increases from 0.025 to 0.2. This behavior, however, is not accurately predicted by the reported $G'_{L_{+}}$ measure, which decreases from 1268 to 1163 kPa, as the strain amplitude is increased from 0.1 to 0.2. Moreover, the

reported measures $G'_{M_{\pm}}$ cannot uniquely characterize the inter-cycle strain amplitude softening phenomenon. As seen in Table 2, $G'_{M_{-}}$ converges to a physically implausible negative value for the minimum strain modulus of MAEs under the strain amplitude of 0.2. The proposed nonlinear measure E'_{DZSM_0} , on the other hand, predicts the zero-strain modulus of 52 kPa under the same strain input. Similarly, the reported measures $\eta'_{M_{\pm}}$ yield two

Table 4 Coefficients of Fourier series and Chebyshev polynomials approximations of the stress response for the unaligned MAE samples under LAOA loading ($\varepsilon_0=0.1$ and 0.2 , $f=1$ Hz, and $B=750$ mT)

Strain amplitude	Coefficients of Fourier series (kPa)							
	E'_1	E''_1	E'_2	E''_2	E'_3	E''_3	E'_4	E''_4
0.1	953	734	136	-126	-152	-61	-17.6	37
0.2	660	579	221	-206	-202	-100	-46	95
	Coefficients of Chebyshev polynomials (kPa)							
	e_1	v_1	e_2	v_2	e_3	v_3	e_4	v_4
0.1	953	117	22.4	-16.5	152	-9.7	1.6	5.6
0.2	660	92	7.8	-31.5	202.4	-16	1.8	14.7

different values for the minimum rate dynamic viscosity, as seen in Table 3. The proposed nonlinear measure corresponding to zero strain-rate, η'_{DZSRV_0} , on the other hand, provides a single value, thereby suggesting a unique interpretation of viscous nonlinearity (e.g., shear-rate thinning).

The quantitative comparisons can be also graphically seen in Figs. 7 and 8. These figures present the Lissajous stress-strain and stress-strain-rate responses, as examples, for the unaligned MAE samples subject to LAOA loading. The first harmonic moduli E'_1 and η'_1 are also shown in Figs. 7 and 8 for comparisons. It can be seen that an increase in strain amplitude from 0.1 to 0.2 yields a local intra-cycle nonlinearity during extension and compression, namely, down-turn strain softening and up-turn strain stiffening. Both the material measures, E'_{DLSM-} and G'_{L-} , predict quite similar values for the down-turn strain softening during extension. The general elastic measure (G'_{L+}), reported by Ewoldt [30], however underestimates the up-turn strain stiffening value during compression, as seen in red circled region in Fig. 8a.

Both the nonlinear elastic measures ($E'_{DLSM\pm}$, $G'_{L\pm}$), however, reduce to linear first harmonic modulus (E'_1) in the linear regime, where the response is linear and symmetric. The results in Tables 2 and 3, and Figs. 7 and 8 suggest that the reported nonlinear measures, $G'_{M\pm}$ and $\eta'_{M\pm}$ [30], cannot predict unique values for the modulus and viscosity for the zero loading condition. Moreover, under the higher strain amplitude of 0.2, the measure G'_{M-} predict physically implausible negative value for minimum strain modulus. In contrast, the proposed nonlinear measures at the zero-loading condition (E'_{DZSM_0} and η'_{DZSRV_0}) possess unique values for zero strain modulus and zero-strain rate dynamic

viscosity. The proposed measures thus permit unique interpretations of inter/intra-cycle nonlinearities. It is also worth mentioning that unlike the slope of loading/unloading paths of the total stress, the proposed measures, $E'_{DLSM\pm}$, and $\eta'_{DLSRV\pm}$, were deliberately chosen as slopes of the equivalent nonlinear elastic stress, and viscous stress, respectively, near peak strain in compression and extension. The convergence of both the measures to the linear strain-independent elastic modulus ($E'_1(\omega)$) and dynamic viscosity ($\eta'_1(\omega)$) at small strains, was further ensured.

Table 4 presents coefficients of the stress response of MAE samples approximated by the Fourier series and the Chebyshev Polynomials. The results are presented for the unaligned MAE samples subject to two different strain amplitudes ($\varepsilon_0=0.1$ and $\varepsilon_0=0.2$) at a frequency of 1 Hz and 750 mT magnetic flux density, as an example. The results show that the first-order elastic modulus (E'_1) estimated from Fourier series is identical to the first-order Chebyshev elastic modulus (e_1), for both the strain amplitudes considered. The magnitudes of the third coefficients (E'_3 and e_3) are identical, while the signs are opposite. This has also been observed in nonlinear responses of viscoelastic materials under LAOS loading [31]. Analysis of Table 3 further implies that the zero strain moduli (E'_{DZSM_0}) and zero strain-rate viscosity (η'_{DZSRV_0}) can be also obtained by taking the average of the minimum strain moduli ($G'_{M\pm}$) and the minimum rate dynamic viscosity ($\eta'_{M\pm}$). This can be noted from Eqs. 16 and 18, as well as Eqs. 45 & 53. Furthermore, this is schematically shown in Fig. 4, given the fact that the Chebyshev viscoelastic stress can be simply considered as mean of the Fourier viscoelastic stress at any instance of input strain. In Sect. 4.3, a set of equivalent Fourier coefficients was established and is summarized in Table 1 to realize the same nonlinear analysis

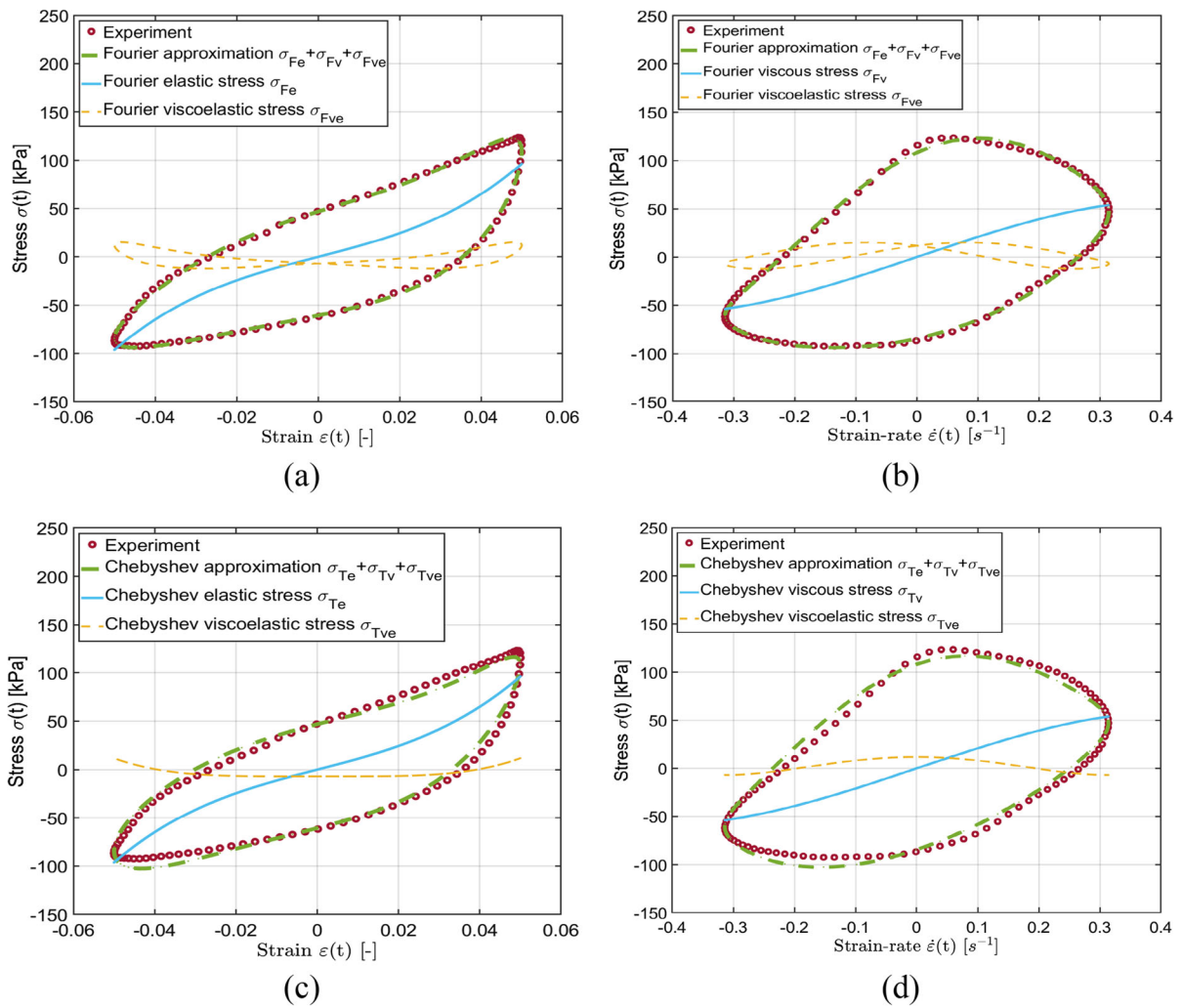


Fig. 9 Stress- strain (left column) and stress–strain-rate (right column) response curves of aligned MAEs obtained from measured data and Fourier **a, b** and Chebyshev **c, d** approximations ($\epsilon_0 = 0.05$, $B=750$ mT, and $f=1$ Hz)

provided above in a faster manner, irrespective of loading conditions. As an example, for the strain amplitude of 0.1, E_2'' equals to $(\omega v_2 - e_2)$ considering the determined coefficients presented in Table 4. This equality is expected given the proposed relationship between coefficients of Fourier series and Chebyshev polynomials (see Table 1).

5 Results and discussion

The measured data are used to derive Fourier and Chebyshev polynomial approximations of elastic-dominated stress responses of MAE samples subject

to LAOA excitations. The stress response approximations using the Fourier series and Chebyshev polynomials are presented together with the elastic, viscous and viscoelastic components as function of the strain and strain rate. The approximated stress responses are subsequently used to determine the proposed measures, $E'_{DLSM\pm}$ and $\eta'_{DLSRV\pm}$. The maximum number of harmonics is limited to four ($n=4$) for the analyses, while the measured stress response has been adjusted for pre-stress due to the pre-strain in order to eliminate the effect of mean stress ($n = 0$). As an example, Figs. 9 and 10 present stress responses of the aligned MAE sample subject to LAOA loading considering two levels of strain amplitude, 0.05 and 0.20,

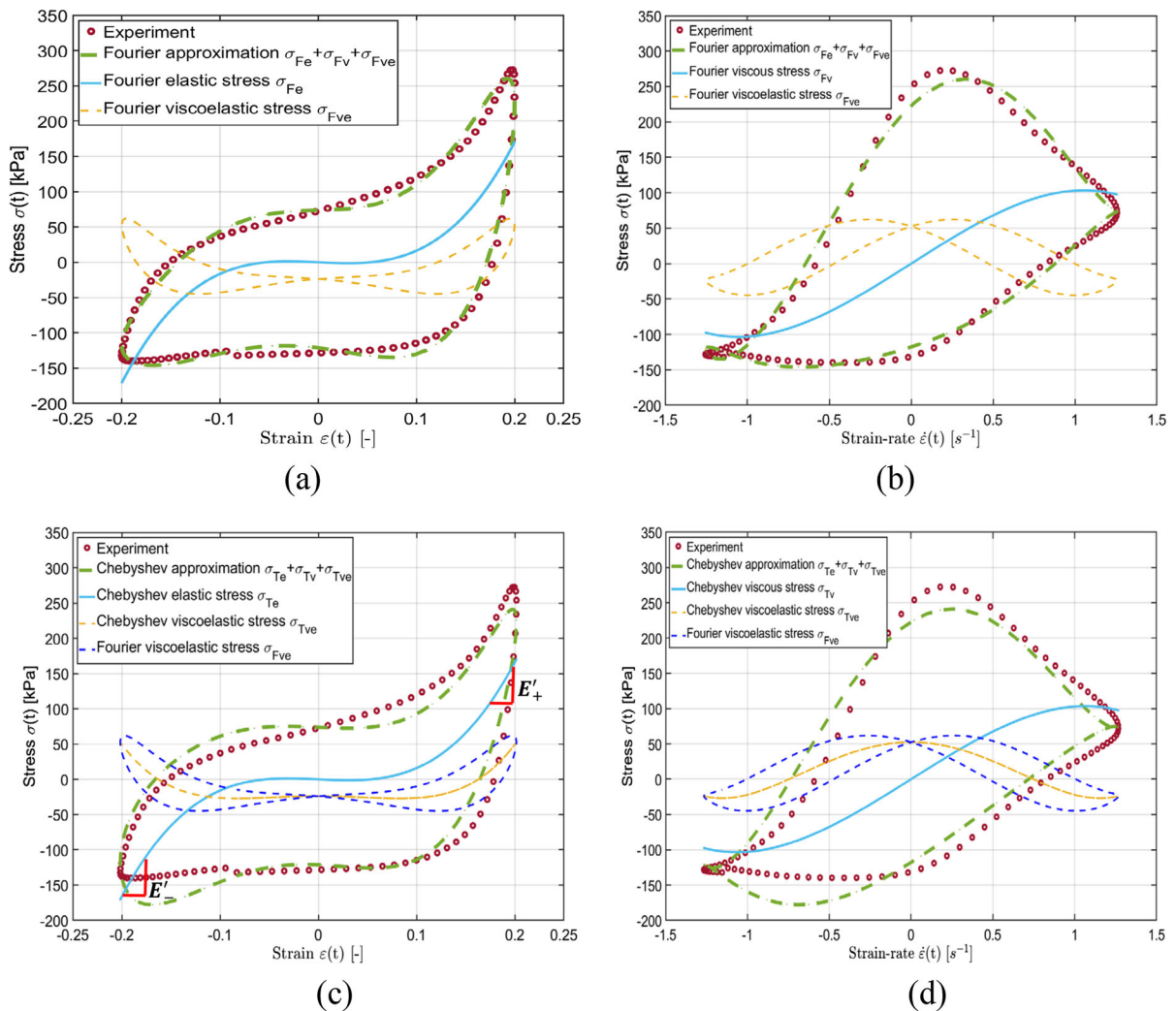


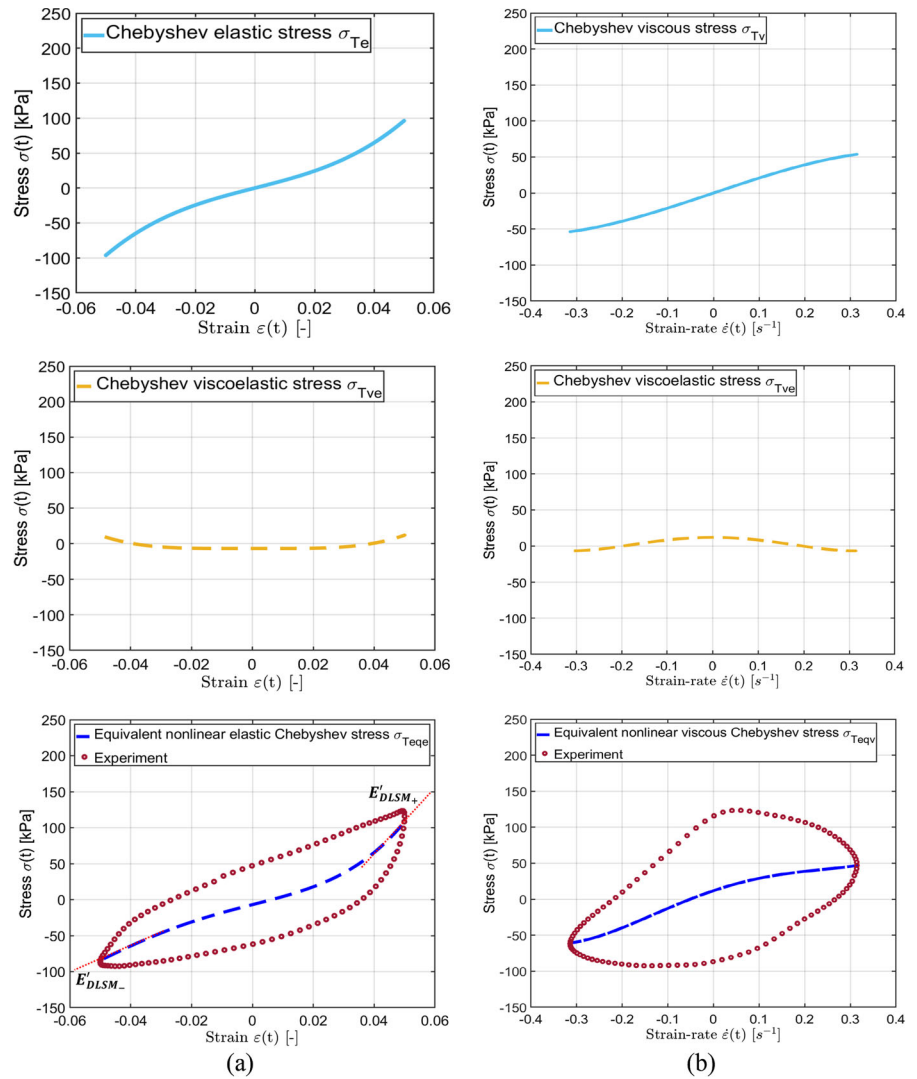
Fig. 10 Stress–strain (left column) and stress–strain-rate (right column) response curves of aligned MAEs obtained from measured data and Fourier **a, b** and Chebyshev **c, d** approximations ($\varepsilon_0 = 0.20$, $B=750$ mT, and $f=1$ Hz)

respectively. The left and right columns in these figures illustrate stress–strain and stress–strain rate responses, respectively. The results in Figs. 9 and 10 are presented for the loading frequency of 1 Hz, and magnetic flux density of 750mT, as an example. Although, the asymmetry in stress responses about zero stress is evident under both levels of strain inputs, the asymmetry becomes far more pronounced as the strain amplitude increases from 0.05 to 0.20. The asymmetric properties of MAEs under LAOA loading are in part due to different microstructural evolution and deformation mechanism in compression and extension [25, 31]. The area bounded by the stress–strain curve during compression ($\varepsilon(t) > 0$) tends to be

considerably greater than that in extension ($\varepsilon(t) < 0$), particularly under higher strain amplitude. This implies that material dissipates more energy during compression than in extension, as seen in Fig. 9.

From the results, it is evident that the elastic and viscous stress components are odd functions of input strain and strain-rate, respectively, while the viscoelastic stress component is an even function of strain and strain-rate, as expected, according to Eqs. (23) and (36). It is also seen that the elastic stress approximated by the Fourier series and Chebyshev polynomials is not able to predict the asymmetric strain–stress characteristics of MAEs. The estimated responses thus yield identical tangential/differential large strain

Fig. 11 Comparison of equivalent nonlinear elastic and viscous Chebyshev stresses of aligned MAE samples with respect to **a** strain and **b** strain-rate ($\epsilon_0 = 0.05$, $B=750$ mT, and $f=1$ Hz)

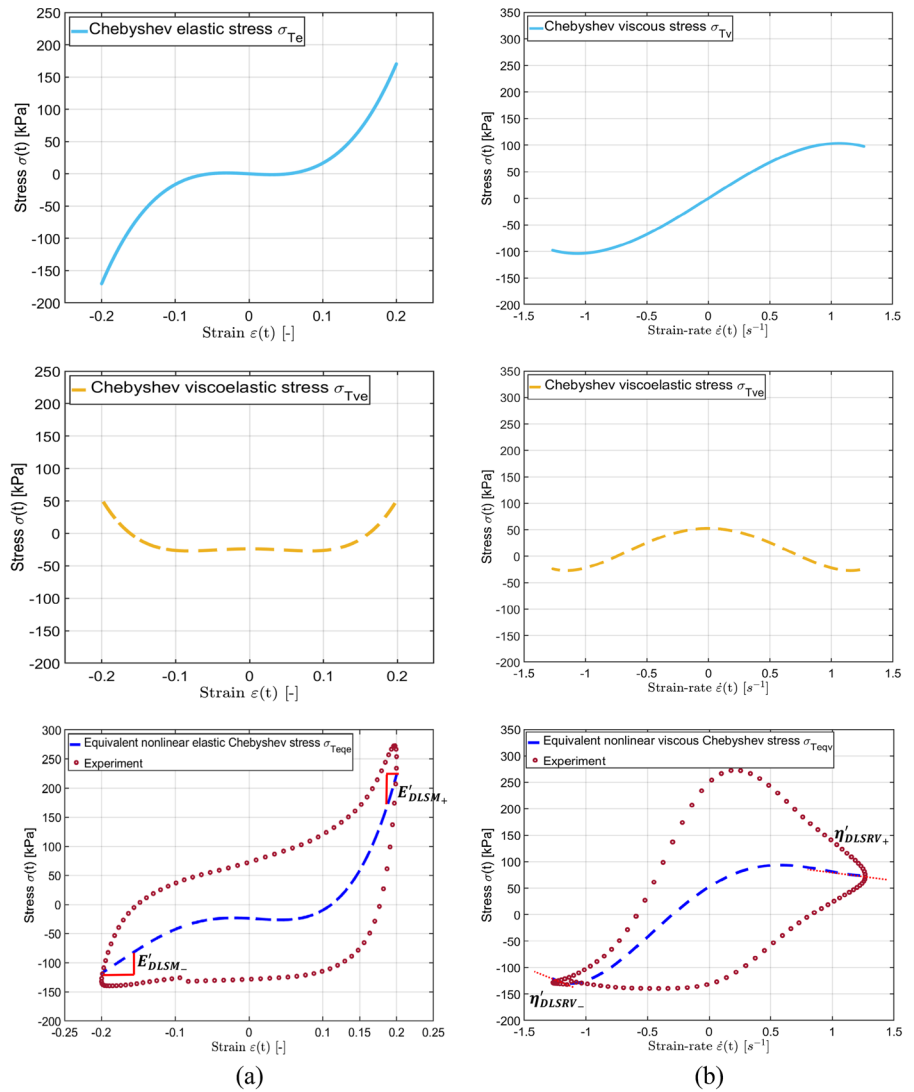


moduli at the end of compression and extension strokes ($E'_- = E'_+$), as seen in Figs. 9c and 10c. Moreover, the area enclosed by the Chebyshev viscoelastic stress component is nearly negligible and substantially smaller than that observed for the Fourier viscoelastic stress, as seen in Fig. 9c and a.

The observed two-fold loop in Fourier viscoelastic response is attributable to the presence of even *sine* terms as seen in Fig. 4. These terms, however, do not exist in the Chebyshev viscoelastic stress response. The closed loop integral of viscoelastic Chebyshev polynomials comprising only even powers of x and y , presented in Eq. (23), thus becomes zero, suggesting negligible energy dissipation. This is also evident in Figs. 9c and 10c.

The results in Fig. 10c show that the Chebyshev viscoelastic stress is close to mean Fourier viscoelastic stress. The Chebyshev viscoelastic stress may thus be considered to represent equivalent elastic stress for the Fourier viscoelastic stress. In a similar manner, Fig. 10d shows that the Chebyshev viscoelastic stress may be considered as an equivalent viscous stress for the Fourier viscoelastic stress. To properly quantify the nonlinearities and asymmetric characteristics of MAEs under LAOA loadings and to further justify the assumption of elastic-dominated behavior of MAEs, we present both equivalent nonlinear elastic and viscous stresses, namely, σ_{Teqe} , and σ_{Teqv} in Figs. 11–12. The σ_{Teqe} can be obtained by superimposing the Chebyshev viscoelastic stress response (σ_{Tve}) to the

Fig. 12 Comparison of equivalent nonlinear elastic and viscous Chebyshev stresses of aligned MAE samples with respect to **a** strain and **b** strain-rate ($\varepsilon_0 = 0.2$, $B=750$ mT, and $f=1$ Hz)



Chebyshev elastic stress responses, σ_{Te} , while the σ_{Teqv} can be derived by superimposing the σ_{Tve} to the Chebyshev viscous stress response, σ_{Tv} (Detailed formulation is presented in Appendix B. Supplementary Data).

Figures 11 and 12 compare the equivalent nonlinear elastic and viscous stresses (σ_{Teqe} , and σ_{Teqv}), respectively, for strain amplitude of 0.05 and 0.20. Figures 11a and 12a show that the σ_{Teqe} more distinctively represents the asymmetry in terms of elastic moduli during compression and extension ($E'_{DLSM+} > E'_{DLSM-}$). This is particularly more evident in Fig. 12a under the higher strain amplitude, where the measure, E'_{DLSM+} , can accurately predict the strain

stiffening at extremity of the compression cycle. This asymmetry, however, is considerably small in the dynamic viscosity measures ($\eta'_{DLSRV+} \cong \eta'_{DLSRV-}$), as seen in Figs. 11b and 12b. It is evident that the assumption of a predominately viscous behavior for MAEs, results in underestimation and implausible negative values for dynamic viscosities ($\eta'_{DLSRV\pm}$) at the minimum and maximum strain-rates, as it is seen in Fig. 12b. This confirms that the nonlinear and asymmetric behavior of MAEs primarily feature the elastic-dominated characteristics, which can be quantified via the proposed differential large strain moduli ($E'_{DLSM\pm}$), presented in Eq. (28). This further suggests that viscoelastic stress response of MAEs predicted by

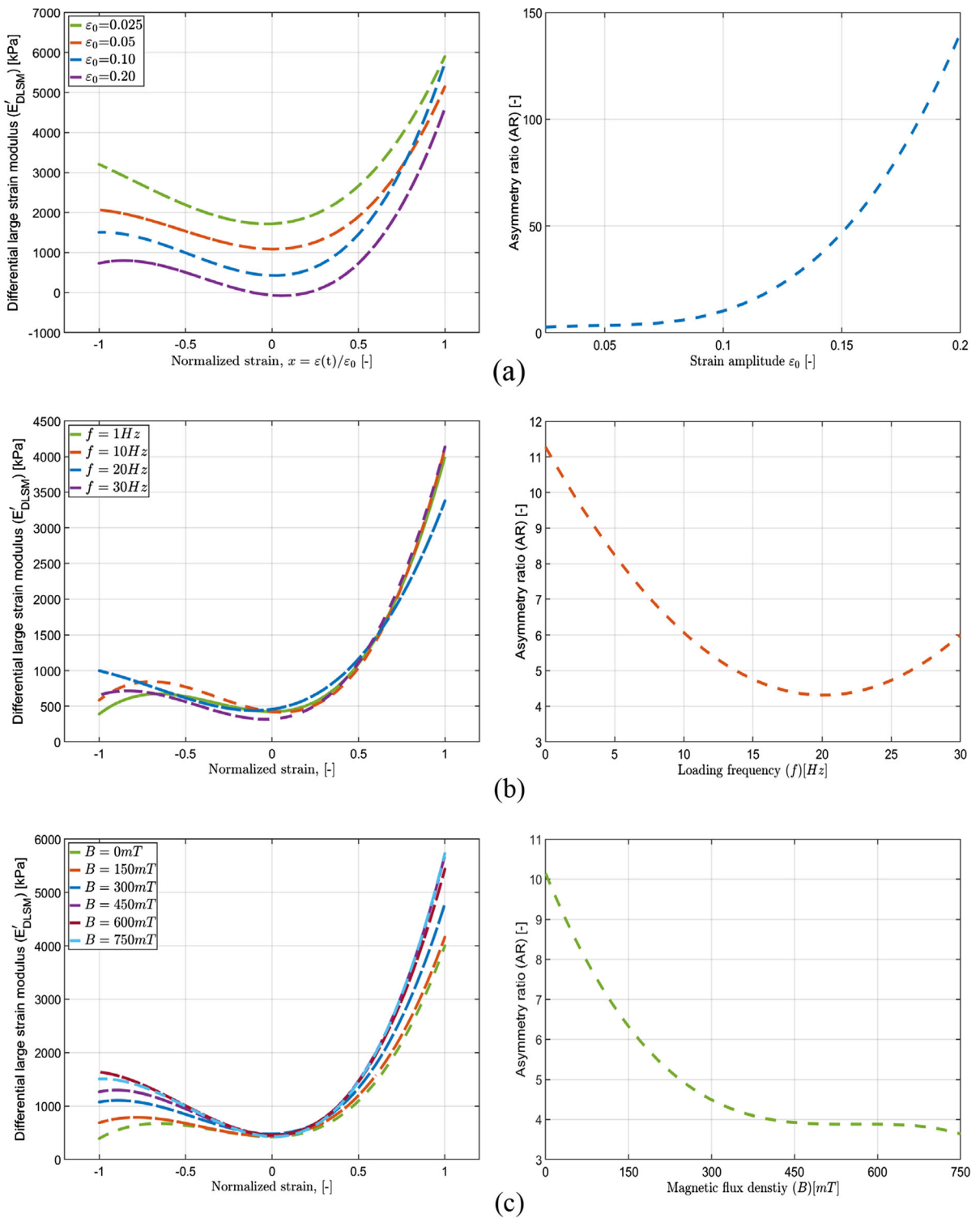


Fig. 13 Variations in proposed differential large strain modulus ($E'_{DLSM\pm}$) obtained for the aligned MAE samples with respect to normalized strain (left column) and the asymmetry

ratio (right column) as functions of strain amplitude, frequency, and magnetic flux density: **a** $f=1$ Hz, $B=750$ mT, **b** $\varepsilon_0=0.1$, $B=0$ mT, and **c** $f=1$ Hz, $\varepsilon_0=0.1$

the Chebyshev polynomial is more elastic-dominated, and supports the assumptions considered in deriving the proposed nonlinear measure (E'_{DLSM}) in Eqs. (25) through (28). Such behavior has also been reported for magneto-rheological elastomeric foams in the dynamic regime, where the viscous behavior was less pronounced as the applied strain increased [55]. It should also be noted that the reasonably good estimates of dynamic viscosity of MAEs, however, can be obtained only from the Chebyshev viscous stress σ_T , (Figs. 11 and 12).

It should be also noted that as opposed to the Chebyshev viscoelastic stress, Fourier viscoelastic stress cannot be simply superimposed to Fourier elastic/viscous stress to yield equivalent elastic/viscous stress. It is because the Fourier viscoelastic stress provides two values for each instant of input strain due to presence of even *Sine* terms as presented in Fig. 4, thereby impeding uniquely quantifying material non-linearity under LAOA loading.

Figure 13 illustrates the variations in the proposed local measure E'_{DLSM} and asymmetry ratio ($AR_{+/-}^e$) obtained from measured characteristics of the MAE samples subject to LAOA loading considering wide ranges of magneto-mechanical conditions. Results in Fig. 13a show relatively higher $E'_{DLSM\pm}$ moduli under the lower strain amplitudes (e.g., $\varepsilon_0=0.025$) when compared to those under the higher strain amplitudes (i.e., $\varepsilon_0=0.2$). This is due to inter-cycle strain-softening of the MAEs. This phenomenon, referred to as Payne effect, has been widely reported in elastomeric materials when elastic/storage modulus decreases with increasing the amplitude of deformation (e.g., [56]). It is also evident that the inter-cycle asymmetry ratio ($AR_{+/-}^e \Big|_{\varepsilon_{02}/\varepsilon_{01}}$) increases with increasing the strain amplitude. Results also show local inter-cycle strain amplitude stiffening during compression. For instance, as can be seen from Fig. 13a, E'_{DLSM+} increases from 5144 to 5732 kPa, when strain amplitude increases from 0.05 to 0.1. This local inter-cycle strain amplitude stiffening during compression may be consistent with the hypothesis that individual long molecular chains in polymeric materials may be stiffened during compression [28]. A further increase in strain amplitude from 0.1 to 0.2 causes the local inter-cycle strain amplitude softening effect at the end of compression cycle to exceed the inter-cycle strain

amplitude stiffening effect. This leads to reduction in the local storage moduli at the end of the compression cycle, from 5732 to 4601 kPa. Although the results are presented for the excitation frequency of 1 Hz, similar trends were also observed for other loading frequencies. Moreover, same trends were also evident for different levels of magnetic flux density. However, for the unaligned MAE samples the inter-cycle strain amplitude stiffening were consistently observed in both ranges of strain amplitude increments (0.05 to 0.1) and (0.1 to 0.2), as noted in Table B.1, Appendix B. Supplementary Data. This is partly attributable to lower sensitivity of unaligned MAEs to strain amplitude softening as compared to aligned MAEs [32].

Figure 13b demonstrates the variations in E'_{DLSM} with normalized strain in the 1 Hz to 30 Hz frequency range. Results generally show a reduction in the asymmetry ratio ($AR_{+/-}^e$) when the loading frequency increased from 1 to 30 Hz. For instance, the E'_{DLSM+} for the loading frequency of 1 Hz and 30 Hz equals to 4002 kPa and 4136 kPa, respectively, and E'_{DLSM-} equals to 390 kPa and 655 kPa, accordingly, corresponding to $AR_{+/-}^e$ of 10.26 and 6.31, respectively. The $AR_{+/-}^e$ generally decreases with increasing frequency due to the inter-cycle strain-rate stiffening behavior of MAEs. However, apart from a slight increase in ($AR_{+/-}^e$) when frequency increased from 20 to 30 Hz, experimental data for other loading conditions generally showed decreasing trends in ($AR_{+/-}^e$) as frequency increased.

Considering the $AR_{+/-}^e$ values at 1 Hz and 30 Hz together with the domains of nonlinearity described in Sect. 4.4.2, this inter-cycle nonlinearity can be descriptively referred to as elastic strain-rate symmetric behavior with increasing frequency ($AR_{+/-}^e \Big|_{\omega_2/\omega_1} = \frac{6.31}{10.26} < 1$). Results in Fig. 13a and b show that the E'_{DLSM} is considerably more sensitive to strain amplitude than the loading frequency. Similar tendencies were also observed under other excitation conditions, including the magnetic flux density and strain amplitude.

Figure 13c illustrates the variations in E'_{DLSM} as a function of normalized strain for magnetic flux density ranging from 0 to 750 mT. It can be observed that the asymmetry ratio, $AR_{+/-}^e$, decreases as the magnetic flux density increases from 0 to 750 mT, while the

E'_{DLSM} increases with magnetic flux density. For instance, the E'_{DLSM+} increases from 4002 and 5732 kPa as flux density increases from 0 to 750 mT, while the correspond increase in E'_{DLSM-} is from 390 to 1506 kPa. These correspond to $AR_{+/-}^e$ of 10.26 and 3.82 for the magnetic flux density of 0 mT and 750 mT, respectively. According to Sect. 4.4.2, this inter-cycle nonlinearity can be referred to as an elastic field-symmetric behavior with increasing magnetic flux density ($AR_{+/-}^e \Big|_{B_2/B_1} = \frac{3.82}{10.26} < 1$). This phenomenon is mainly due to the fact that the effect of strain on asymmetry-stiffening of MAEs during compression and extension is more significant when the material is quite soft under zero-field. Owing to the magnetic field stiffening effect of MAEs, the material becomes highly stiff, which leads to lesser asymmetry in compression than in extension. The E'_{DLSM} , however, is more sensitive to strain amplitude as compared with magnetic flux density, as seen from Fig. 13a and c. Similar trends were also observed for other loading frequencies and strain amplitudes.

It should be noted that the proposed nonlinear measures were determined under other loading conditions for both unaligned and aligned MAEs and presented in Appendix C. Supplementary Data. For instance, Table C.1 and C.2 summarize the nonlinear measures at the extremities of the compression and extension cycles ($E'_{DLSM\pm}$), respectively, for unaligned and aligned MAE samples. Tables C.3 and C.4 present the materials moduli at zero strain (E'_{DZSM0}), respectively, for unaligned and aligned MAE samples. Analysis of Tables C.1 and C.2 further shows that the nonlinear measures at extension extremities (E'_{DLSM-}) become negative at only very large strain amplitude of 0.20. This is expected due to following facts: (i) the contribution of nonlinearities of viscoelastic Chebyshev stress is significant, apart from elastic and viscous nonlinearities and (ii) the nonlinear measures at the extremities of the compression and extension cycles ($E'_{DLSM\pm}$) are derived upon assumption that the MAE samples possess highly elastic behavior, and thus their corresponding Chebyshev viscoelastic stress is fully contributed to Chebyshev elastic stress to obtain the equivalent nonlinear Chebyshev stress as presented in Eq. (24). In other words, by assigning the total Chebyshev viscoelastic stress component to elastic component, the nonlinear

elastic behavior is slightly overestimated, and some part of the Chebyshev viscoelastic stress must have contributed to viscous nonlinearity. For instance, according to Fig. 12a, it is possible that the negative slope of Chebyshev viscoelastic stress at large amplitude in extension become large and exceeds the positive slope of the elastic stress at end of extension cycle, thereby leading to slightly negative value of E'_{DLSM-} .

Furthermore, analysis of nonlinear measures for MAEs at zero strain show that the values of E'_{DZSM0} are positive. Nonetheless, only for aligned MAE samples under higher level of magnetic flux densities ($B \geq 600mT$), the values of E'_{DZSM0} become slightly negative as presented in Table C.4 in Appendix C. Supplementary Data. It is partly attributed to the magnetic field-stiffening of the MAEs that limits recovery or unloading of the specimen during experiment. It can also be seen in Fig. 8a that the slope of unloading path in stress–strain curve around zero strain slightly changes and becomes negative.

6 Conclusions

MAEs subject to large amplitude oscillatory loading in the axial direction (LAOA) exhibit highly nonlinear and asymmetric stress–strain characteristics. Proposed differential large strain modulus ($E'_{DLSM\pm}$) and differential large strain-rate viscosity ($\eta'_{DLSRV\pm}$) measures provided accurate estimations of material's moduli in compression and extension, and thereby the asymmetric stress–strain responses of MAEs to LAOA loadings. The proposed nonlinear measures at zero strain and zero strain-rate, E'_{DZSM0} , and η'_{DZSRV0} , also provided unique values of slopes, while the conventional minimum strain measures ($G'_{M\pm}$, $\eta'_{M\pm}$) lead to two different values. The proposed measures thus permitted unique interpretations of inter-cycle nonlinearities of MAEs subject to LAOA loadings. The stress responses approximated using Fourier series and Chebyshev polynomials permitted decompositions into elastic, viscous, and viscoelastic stress components. Results showed that Chebyshev viscoelastic component can be considered as the equivalent elastic stress of Fourier viscoelastic component. The equivalent elastic and viscous stresses may thus be estimated by superimposing the Chebyshev

viscoelastic and elastic or viscous components, depending on whether the material's response is elastic- or viscous-dominated. Results suggested elastic-dominated responses of MAEs under LAOA loading. The proposed nonlinear elastic measures, i.e., $E'_{DLSM\pm}$ and E'_{DZSM0} , could thus be derived from derivative of the equivalent nonlinear elastic Chebyshev stress with respect to the imposed strain. An equivalent set of Fourier coefficients, obtained in the study, could yield the equivalent nonlinear elastic/viscous stress, enabling faster calculations of the nonlinear measures. It is shown that the proposed local measures together with the asymmetry ratios provide unique interpretations of inter-cycle (e.g., strain amplitude softening and strain amplitude stiffening) and intra-cycle (e.g., strain stiffening) nonlinearities of MAEs under LAOA loadings. The asymmetry ratios in view of elastic modulus ($AR_{+/-}^e$) increased considerably with increasing strain amplitude but decreased with increase in loading frequency and magnetic flux density. The proposed measures together with the quantification methodology could provide enhanced understanding of nonlinear and asymmetric response characteristics of MAEs subject to LAOA loadings. The proposed measures could also facilitate relative analyses of response behaviors of MAEs in the LAOA regime with greater sensitivity near extremities of compression and extension strokes.

Funding Open Access funding provided by National Research Council Canada. This work was supported in part by the Natural Sciences and Engineering Research Council of Canada (NSERC) and in part by the Concordia University Horizon Postdoctoral Fellowship.

Data availability The datasets generated during and/or analyzed during the current study are available from the corresponding author on reasonable request.

Declarations

Conflict of interest The authors declare that there is no conflict of interests regarding the publication of this paper.

Open Access This article is licensed under a Creative Commons Attribution 4.0 International License, which permits use, sharing, adaptation, distribution and reproduction in any medium or format, as long as you give appropriate credit to the original author(s) and the source, provide a link to the Creative Commons licence, and indicate if changes were made. The images or other third party material in this article are included in the article's Creative Commons licence, unless indicated otherwise in a credit line to the material. If material is not included in the article's Creative Commons licence and your intended use is not permitted by statutory regulation or exceeds the permitted use, you will need to obtain permission directly from the copyright holder. To view a copy of this licence, visit <http://creativecommons.org/licenses/by/4.0/>.

Appendix A

See Figs. A1 and A2.

Fig. A1 Stress–strain characteristics of unaligned MAEs subject to different amplitudes of axial strain at a frequency of 1 Hz: **a** $\varepsilon_0=0.025$, **b** $\varepsilon_0=0.10$, and **c** $\varepsilon_0=0.20$. (Magnetic flux density = 0 mT, left column; and = 750 mT, right column)

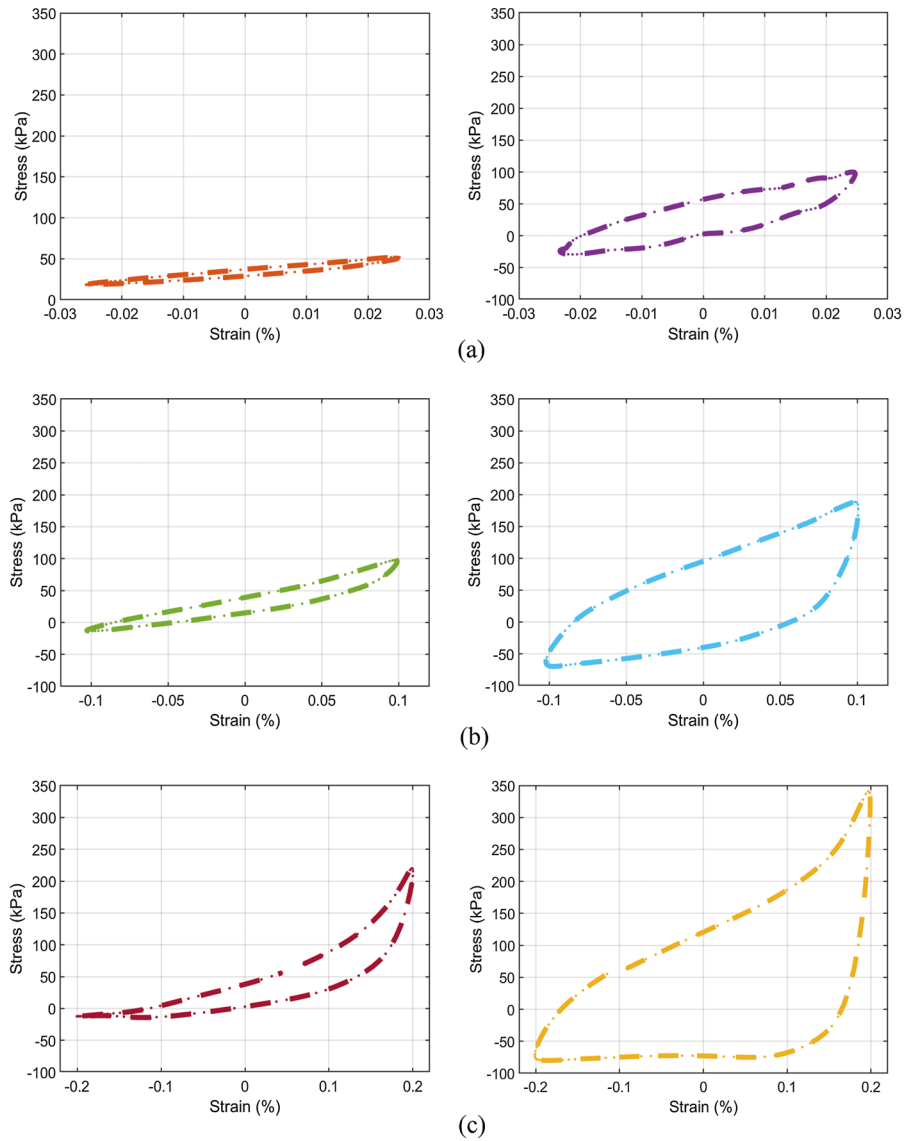
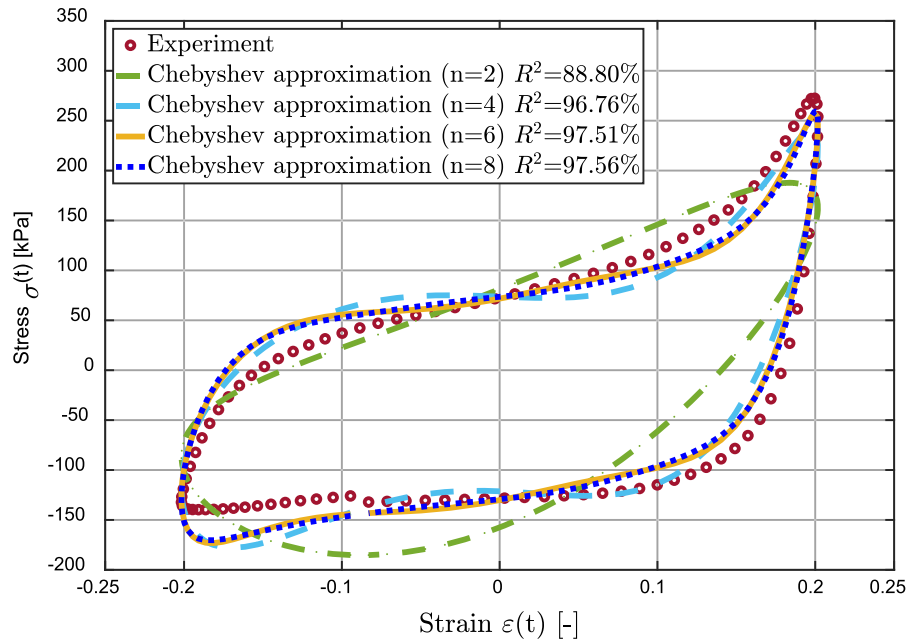


Fig. A2 First-, second-, third-, and fourth-order Chebyshev stress approximations of the measured stress–strain characteristics of aligned MAEs subjected to axial strain at a frequency of 1 Hz, strain amplitude of $\varepsilon_0=0.20$, and magnetic flux density of 750 mT



Appendix B

In case of a viscous-dominated situation, an equivalent nonlinear viscous Chebyshev stress could be obtained from:

$$\sigma_{T_{eqv}}(x) = \sigma_{Tv}(y) + \sigma_{Tve}(x, y) \tag{B.1}$$

In this case, the viscoelastic Chebyshev coefficients are completely contributed to the viscous nonlinearities and asymmetries. Thus, the $\eta'_{DLSRV_{\pm}}$ can be determined, as:

$$\eta'_{DLSRV_{\pm}} = \left. \frac{d\sigma_{T_{eqv}}}{d\dot{\varepsilon}} \right|_{\dot{\varepsilon}=\pm\varepsilon_0\omega} \tag{B.2}$$

The $\eta'_{DLSRV_{\pm}}$ may be expanded for in compression (+) and extension (-) considering $n= 2$, and $n= 4$, as:

$$\begin{aligned} \eta'_{DLSRV_{\pm}} &= \left. \frac{d\sigma_{T_{eqv}}}{d\dot{\varepsilon}} \right|_{\dot{\varepsilon}=\pm\varepsilon_0\omega} = \left. \frac{d\sigma_{T_{eqv}}}{\varepsilon_0\omega dy} \right|_{y=\pm 1; n=2} \\ &= [v_1] \pm 4[(v_2) \mp \frac{1}{\omega}(e_2)] \end{aligned} \tag{B.3}$$

$$\begin{aligned} \eta'_{DLSRV_{\pm}} &= \left. \frac{d\sigma_{T_{eqv}}}{d\dot{\varepsilon}} \right|_{\dot{\varepsilon}=\pm\varepsilon_0\omega} = \left. \frac{d\sigma_{T_{eqv}}}{\varepsilon_0\omega dy} \right|_{y=\pm 1; n=4} \\ &= [v_1 + 9v_3] \pm 4[(v_2 + 4v_4) \mp \frac{1}{\omega}(e_2 - 4e_4)] \end{aligned} \tag{B.4}$$

Similarly, the differential zero strain-rate viscosity (η'_{DZSRV_0}) can be obtained as:

Table B.1 Relationship between coefficients of Fourier series and Chebyshev polynomials for viscoelastic materials exhibiting viscous- and elastic-dominated behavior under LAOA loading ($n = 4$)

Coefficients	Viscoelastic materials exhibiting viscous-dominated response							
	v_1	v_2	v_3	v_4	e_1	$e_{2\pm}$	e_3	e_4
Fourier	E''_1/ω	$0.99E''_2/\omega$	$0.97E''_3/\omega$	$0.95E''_4/\omega$	E'_1	$\mp 3.40E'_2$	$-E'_3$	$1.5E'_4$
Coefficients	Viscoelastic materials exhibiting elastic-dominated response							
	v_1	v_2	v_3	v_4	e_1	$e_{2\pm}$	e_3	e_4
Fourier	E''_1/ω	$0.99E''_2/\omega$	E''_3/ω	$0.95E''_4/\omega$	E'_1	$\mp 3.40E'_2$	$-0.97E'_3$	$1.5E'_4$

$$\eta'_{DZSRV_0} = \left. \frac{d\sigma_{T_{eqv}}}{d\dot{\varepsilon}} \right|_{\dot{\varepsilon}=0;n=2} = \left. \frac{d\sigma_{T_{eqv}}}{\varepsilon_0\omega dy} \right|_{y=0;n=2} = \nu_1 \tag{B.5}$$

$$\eta'_{DZSRV_0} = \left. \frac{d\sigma_{T_{eqv}}}{d\dot{\varepsilon}} \right|_{\dot{\varepsilon}=0;n=4} = \left. \frac{d\sigma_{T_{eqv}}}{\varepsilon_0\omega dy} \right|_{y=0;n=4} = \nu_1 - 3\nu_3 \tag{B.6}$$

An equivalent nonlinear viscous Fourier stress can also be defined for the case of viscous-dominated situation as:

$$\sigma_{F_{eqv}}(x, y) = \sigma_{F_V}(y) + \sigma_{F_{ve}}(x, y) \tag{B.7}$$

The $\eta'_{DLSRV_{\pm}}$ can determined in a similar manner as:

$$\eta'_{DLSRV_{\pm}} = \left. \frac{d\sigma_{F_{eqv}}}{d\dot{\varepsilon}} \right|_{\dot{\varepsilon}=\pm\varepsilon_0\omega} = \left. \frac{d\sigma_{F_{eqv}}}{\varepsilon_0\omega dy} \right|_{y=\pm 1} \tag{B.8}$$

Similarly, $\eta'_{DLSRV_{\pm}}$ can also be expanded for compression (+) and extension (-) considering $n= 2$, and $n= 4$, as:

$$\begin{aligned} \eta'_{DLSRV_{\pm}} &= \left. \frac{d\sigma_{F_{eqv}}}{d\dot{\varepsilon}} \right|_{\dot{\varepsilon}=\pm 0.99\varepsilon_0\omega} = \left. \frac{d\sigma_{F_{eqv}}}{\varepsilon_0\omega dy} \right|_{y=\pm 0.99;n=2} \\ &= \frac{1}{\omega} [(E''_1 \pm 3.96E''_2) - 13.61E'_2] \end{aligned} \tag{B.9}$$

$$\begin{aligned} \eta'_{DLSRV_{\pm}} &= \left. \frac{d\sigma_{F_{eqv}}}{d\dot{\varepsilon}} \right|_{\dot{\varepsilon}=\pm 0.99\varepsilon_0\omega} = \left. \frac{d\sigma_{F_{eqv}}}{\varepsilon_0\omega dy} \right|_{y=\pm 0.99;n=4} \\ &= \frac{1}{\omega} [E''_1 + 8.76E''_3] + \frac{1}{\omega} [-13.61E'_2 \\ &\quad - 23.93E'_4 \pm 3.96E''_2 \pm 15.21E''_4] \end{aligned} \tag{B.10}$$

The differential zero strain-rate viscosity (η'_{DZSRV_0}) can also be obtained in a similar manner, as:

$$\eta'_{DZSRV_0} = \left. \frac{d\sigma_{F_{eqv}}}{d\dot{\varepsilon}} \right|_{\dot{\varepsilon}=0;n=2} = \frac{1}{\omega} [E''_1 + 2E'_2] \tag{B.11}$$

$$\begin{aligned} \eta'_{DZSRV_0} &= \left. \frac{d\sigma_{F_{eqv}}}{d\dot{\varepsilon}} \right|_{\dot{\varepsilon}=0;n=4} \\ &= \frac{1}{\omega} [E''_1 - 3E''_3 + 2E'_2 - 4E'_4] \end{aligned} \tag{B.12}$$

Apart from $\eta'_{DLSRV_{\pm}}$, differential large strain moduli ($E'_{DLSM_{\pm}}$) can be defined for the Chebyshev and Fourier elastic stress components for materials showing viscous-dominated behavior, as:

$$E'_{DLSM_{\pm}} = \left. \frac{d\sigma_{T_e}}{d\varepsilon} \right|_{\varepsilon=\pm\varepsilon_0} \tag{B.13}$$

$$E'_{DLSM_{\pm}} = \left. \frac{d\sigma_{F_e}}{d\varepsilon} \right|_{\varepsilon=\pm\varepsilon_0} \tag{B.14}$$

Considering $n = 4$, as an example, $E'_{DLSM_{\pm}}$ can be obtained as:

$$E'_{DLSM_{\pm}} = \left. \frac{d\sigma_{T_e}}{d\varepsilon} \right|_{\varepsilon=\pm\varepsilon_0;n=4} = e_1 + 9e_3 \tag{B.15}$$

$$E'_{DLSM_{\pm}} = \left. \frac{d\sigma_{F_e}}{d\varepsilon} \right|_{\varepsilon=\pm\varepsilon_0;n=4} = E'_1 - 9E'_3 \tag{B.16}$$

In order to quantify inter/intra-cycle nonlinearities (e.g., strain stiffening and strain softening) in viscoelastic materials showing viscous-dominated behavior, the differential zero strain modulus (E'_{DZSM_0}) can also be defined for their Chebyshev and Fourier elastic stress responses as:

$$E'_{DZSM_0} = \left. \frac{d\sigma_{T_e}}{d\varepsilon} \right|_{\varepsilon=0} \tag{B.17}$$

$$E'_{DZSM_0} = \left. \frac{d\sigma_{F_e}}{d\varepsilon} \right|_{\varepsilon=0} \tag{B.18}$$

Considering $n = 4$, as an example, E'_{DZSM_0} can be obtained from σ_{T_e} and σ_{F_e} , given by:

$$E'_{DZSM_0} = \left. \frac{d\sigma_{T_e}}{d\varepsilon} \right|_{\varepsilon=0;n=4} = e_1 - 3e_3 \tag{B.19}$$

$$E'_{DZSM_0} = \left. \frac{d\sigma_{F_e}}{d\varepsilon} \right|_{\varepsilon=0;n=4} = E'_1 + 3E'_3 \tag{B.20}$$

Unlike Eq. (B.2), where $\eta'_{DLSRV_{\pm}}$ is determined from taking derivative of the equivalent nonlinear viscous stress obtained via Chebyshev polynomials for $y = \pm 1$, the $\eta'_{DLSRV_{\pm}}$ in Eqs. (B.9) and (B.10) must be obtained for when $y \neq \pm 1$ (e.g., $y = \pm 0.99$) to eliminate singularities. It should be noted that the value of $\eta'_{DLSRV_{\pm}}$, expressed in Eqs. (B.9) and (B.10), near extremities of the loading cycle becomes highly dependent on how close the y is to 1. As an example, we compare Eqs. (B.3) and (B.4) with Eqs. (B.9) and (B.10), respectively, considering $y = \pm 0.99$, as well as Eqs. (B.15) and (B.16) with Eqs. (B.19) and (B.20), correspondingly. Subsequently, the relationships

between the coefficients of the Fourier series and Chebyshev polynomials can be obtained for viscoelastic materials showing viscous-dominated behavior under LAOA regime. These are shown in Table B.1, considering $n=4$. A suitable value for y , however, needs to be determined in order to derive an explicit relationship between the Fourier coefficients and Chebyshev polynomials.

A similar relation between the Fourier series and Chebyshev polynomials can be also obtained for materials showing elastic dominated behavior by comparing Eqs. (29) and (30) with Eq. (42). These are shown in Table B.1 for $n=4$, as an example.

As already explained in Sect. 4.3, even though an explicit relationship between the coefficients of Fourier and Chebyshev approximations over the entire domain of orthogonality, $[-1,1]$, cannot be derived, equivalent elastic/viscous Chebyshev stress can be obtained from equivalent elastic/viscous Fourier stress by excluding the *sine* terms. This permits faster

calculation of the proposed set of moduli. The $\eta'_{DLSRV_{\pm}}$, presented in Eq. (B.4), can thus also be obtained for in compression (+) and extension (-) considering $n=2$, and 4, as:

$$\eta'_{DLSRV_{\pm}} = \left. \frac{d\sigma_{F'_{eqv}}}{\varepsilon_0 dx} \right|_{x=\pm 1; n=2} = E''_1 + 4E''_2 \tag{B.21}$$

$$\eta'_{DLSRV_{\pm}} = \left. \frac{d\sigma_{F'_{eqv}}}{\varepsilon_0 dx} \right|_{x=0; n=4} = E''_1 + 4E''_2 + 9E''_3 + 16E''_4 \tag{B.22}$$

$$\eta'_{DZSRV_0} = \left. \frac{d\sigma_{F'_{eqv}}}{\varepsilon_0 dx} \right|_{x=0; n=4} = E''_1 - 3E''_3 \tag{B.23}$$

Appendix C

See Table C.1, C.2, C.3, C.4, C.5 and C.6.

different strain amplitudes (superimposed on pre-strain of 0.21), loading frequency, and magnetic flux density

Table C.1 Differential large strain moduli, $E'_{DLSM_{\pm}}$ (kPa), obtained at the extremities of the compression (+) and extension (-) cycles for unaligned MAE samples subject to

B (mT)	Frequency	$\varepsilon_0=0.025$		$\varepsilon_0=0.05$		$\varepsilon_0=0.1$		$\varepsilon_0=0.2$	
		E'_{DLSM_-}	E'_{DLSM_+}	E'_{DLSM_-}	E'_{DLSM_+}	E'_{DLSM_-}	E'_{DLSM_+}	E'_{DLSM_-}	E'_{DLSM_+}
0	1 Hz	532	1126	333	1005	360	1320	- 376	2657
	10 Hz	537	1303	536	1379	258	1386	- 381	2679
	20 Hz	2350	3318	580	2162	629	2155	-	- *
	30 Hz	- 228	1705	464	1663	492	3201	-	-
	1 Hz	740	1775	806	1605	426	1783	- 551	3202
150	10 Hz	1584	1891	1430	1983	577	1997	- 561	3421
	20 Hz	2215	4161	1763	3883	232	2800	-	-
	30 Hz	512	2374	950	2247	793	3494	-	-
	1 Hz	1566	952	1302	1981	839	2283	- 714	4087
300	10 Hz	1798	3861	1666	3357	850	2998	- 812	4562
	20 Hz	1088	2184	2195	4628	946	3359	-	-
	30 Hz	1746	1949	1865	2980	848	3997	-	-
	1 Hz	2659	3967	1583	2854	853	3164	- 549	5234
450	10 Hz	3821	4568	2207	4526	1511	3730	- 318	5081
	20 Hz	1720	3337	1458	4684	797	4037	-	-
	30 Hz	3418	3632	2434	3826	1243	4435	-	-
	1 Hz	2323	3436	1967	3498	1067	3450	- 158	5285
600	10 Hz	4793	6049	2278	5242	1466	4269	41	5389
	20 Hz	1659	4318	3179	6009	1605	4480	-	-
	30 Hz	2914	5384	2575	4556	1699	4359	-	-
	1 Hz	1639	6887	2191	3312	1231	3460	123	4891

Table C.1 continued

<i>B</i> (mT)	Frequency	$\epsilon_0=0.025$		$\epsilon_0=0.05$		$\epsilon_0=0.1$		$\epsilon_0=0.2$	
		E'_{DLSM-}	E'_{DLSM+}	E'_{DLSM-}	E'_{DLSM+}	E'_{DLSM-}	E'_{DLSM+}	E'_{DLSM-}	E'_{DLSM+}
750	10 Hz	4278	6940	2750	5150	1402	4477	280	5564
	20 Hz	5644	8429	2176	6603	1218	4669	–	–
	30 Hz	2436	4871	2935	4541	1330	5212	–	–

*Performing measurement simultaneously at large amplitudes and high frequencies was not possible

Table C.2 Differential large strain moduli, $E'_{DLSM\pm}$ (kPa), obtained at the extremities of the compression (+) and extension (-) cycles for aligned MAE samples subject to different strain amplitudes (superimposed on pre-strain of 0.21), loading frequency, and magnetic flux density

<i>B</i> (mT)	Frequency	$\epsilon_0=0.025$		$\epsilon_0=0.05$		$\epsilon_0=0.1$		$\epsilon_0=0.2$	
		E'_{DLSM-}	E'_{DLSM+}	E'_{DLSM-}	E'_{DLSM+}	E'_{DLSM-}	E'_{DLSM+}	E'_{DLSM-}	E'_{DLSM+}
0	1 Hz	835	2185	693	2365	390	4002	– 25	3443
	10 Hz	1305	2934	834	2748	585	4122	–	–*
	20 Hz	2951	3012	1650	2723	998	3380	–	–
	30 Hz	320	1643	619	2388	655	4136	–	–
	1 Hz	1552	2187	955	3069	686	4164	– 79	3716
150	10 Hz	1772	4463	1704	3151	1059	4306	–	–
	20 Hz	3585	5393	2419	3981	1311	3925	–	–
	30 Hz	1330	3180	1375	3194	943	5008	–	–
300	1 Hz	1990	3056	1502	3473	1076	4789	80	4204
	10 Hz	3340	5401	1922	4925	1414	5389	–	–
	20 Hz	2825	3945	2950	5003	1849	5028	–	–
	30 Hz	3341	6057	1566	4089	1149	5447	–	–
450	1 Hz	2390	5112	1953	4003	1266	5698	390	4764
	10 Hz	3048	8229	2894	4999	1995	5485	–	–
	20 Hz	5511	8576	2287	4557	1603	5005	–	–
	30 Hz	2614	6849	2027	3827	1634	5125	–	–
600	1 Hz	2904	4986	2114	5111	1637	5436	531	5018
	10 Hz	4934	7958	2301	6734	1908	6334	–	–
	20 Hz	3487	8652	4293	5979	1693	6126	–	–
	30 Hz	2867	7468	2934	4892	2205	4844	–	–
750	1 Hz	3207	5897	2064	5144	1506	5732	731	4601
	10 Hz	4608	7969	3000	6682	2071	6325	–	–
	20 Hz	4415	7886	3128	6319	2573	5936	–	–
	30 Hz	3848	7488	2554	5324	2313	5048	–	–

*Performing measurement simultaneously at large amplitudes and high frequencies was not possible. No error detected.

Table C.3 Differential zero strain moduli, $E'_{DZSM_0}(kPa)$, obtained for unaligned MAE samples subject to different strain amplitudes (superimposed on pre-strain of 0.21), loading frequencies, and magnetic flux densities

B (mT)	Frequency	$\varepsilon_0=0.025$ E'_{DZSM_0}	$\varepsilon_0=0.05$ E'_{DZSM_0}	$\varepsilon_0=0.1$ E'_{DZSM_0}	$\varepsilon_0=0.2$ E'_{DZSM_0}
0	1 Hz	560	511	383	223
	10 Hz	682	543	372	189
	20 Hz	830	831	522	-*
	30 Hz	1010	666	283	-
150	1 Hz	784	583	416	249
	10 Hz	1316	827	506	277
	20 Hz	1146	711	639	-
300	30 Hz	1596	996	372	-
	1 Hz	1350	879	489	265
	10 Hz	1759	1133	627	293
450	20 Hz	2142	929	681	-
	30 Hz	2277	1175	513	-
	1 Hz	1367	1015	528	140
600	10 Hz	2114	1230	666	249
	20 Hz	2847	1572	784	-
	30 Hz	2506	1348	443	-
750	1 Hz	1961	1026	528	54
	10 Hz	2257	1358	709	187
	20 Hz	3015	1254	711	-
	30 Hz	2725	1473	601	-
	1 Hz	1605	1077	496	52
	10 Hz	2327	1354	631	98
	20 Hz	2324	1610	730	-
	30 Hz	2973	1512	524	-

*Performing measurement simultaneously at large amplitudes and high frequencies was not possible

Table C.4 Differential zero strain moduli, $E'_{DZSM_0}(kPa)$, obtained for aligned MAE samples subject to different strain amplitudes (superimposed on pre-strain of 0.21), loading frequencies, and magnetic flux densities

B (mT)	Frequency	$\varepsilon_0=0.025$ E'_{DZSM_0}	$\varepsilon_0=0.05$ E'_{DZSM_0}	$\varepsilon_0=0.1$ E'_{DZSM_0}	$\varepsilon_0=0.2$ E'_{DZSM_0}
0	1 Hz	859	655	422	134
	10 Hz	1022	741	423	-*
	20 Hz	666	566	456	-
	30 Hz	1312	760	318	-
150	1 Hz	1054	755	439	146
	10 Hz	1405	948	540	-
	20 Hz	974	721	536	-
300	30 Hz	1739	981	330	-
	1 Hz	1333	938	476	100
	10 Hz	1802	1084	577	-
450	20 Hz	2175	910	526	-
	30 Hz	1924	1203	380	-
	1 Hz	1504	1061	449	31
600	10 Hz	1949	1296	628	-
	20 Hz	1705	1479	784	-
	30 Hz	2560	1484	409	-
750	1 Hz	1795	1032	457	-40
	10 Hz	2201	1299	618	-
	20 Hz	2219	1120	625	-
	30 Hz	2795	1475	493	-
	1 Hz	1719	1085	426	-66
	10 Hz	2350	1237	493	-
	20 Hz	2807	1409	407	-
	30 Hz	2874	1497	466	-

*Performing measurement simultaneously at large amplitudes and high frequencies was not possible

Table C.5 Differential zero strain-rate viscosity, (+) and extension (-) cycles for unaligned MAE samples η'_{DZSRV_0} (*kPa.s*), and large strain-rate viscosity, subject to different strain amplitudes (superimposed on pre-strain of 0.21), loading frequency, and magnetic flux density $\eta'_{DLSRV_{\pm}}$ (*kPa.s*) obtained at the extremities of the compression

<i>B</i> (mT)	Frequency	$\epsilon_0 = 0.025$		$\epsilon_0 = 0.05$		$\epsilon_0 = 0.1$		$\epsilon_0 = 0.2$	
		η'_{DZSRV_0}	$\eta'_{DLSRV_{\pm}}$	η'_{DZSRV_0}	$\eta'_{DLSRV_{\pm}}$	η'_{DZSRV_0}	$\eta'_{DLSRV_{\pm}}$	η'_{DZSRV_0}	$\eta'_{DLSRV_{\pm}}$
0	1 Hz	26.61	23.63	28.44	5.35	27.30	3.35	37.48	- 35.91
	10 Hz	4.82	0.52	3.22	3.32	2.98	1.93	3.50	- 1.80
	20 Hz	- 0.41	16.19	0.41	8.94	0.89	4.43	-	-
	30 Hz	1.94	0.94	1.91	0.02	2.14	- 0.88	-	-
150	1 Hz	39.33	66.61	51.03	27.46	51.90	7.99	57.87	- 42.42
	10 Hz	5.75	8.00	6.24	4.84	6.02	0.45	3.90	0.97
	20 Hz	5.08	- 4.07	2.37	6.06	2.36	2.35	-	-
300	30 Hz	2.59	1.08	2.99	0.30	2.77	- 1.56	-	-
	1 Hz	74.24	135.50	83.40	80.50	83.99	27.20	85.94	- 50.34
	10 Hz	16.56	3.91	10.56	8.57	8.95	3.45	6.40	0.84
450	20 Hz	5.74	- 0.88	7.33	- 4.71	2.80	3.91	-	-
	30 Hz	5.08	0.46	5.03	- 0.86	4.50	- 2.24	-	-
	1 Hz	138.24	174.41	118.96	136.97	104.62	41.70	105.41	- 37.29
	10 Hz	17.77	19.89	16.01	9.47	12.05	5.16	9.62	- 0.32
600	20 Hz	7.29	8.75	5.02	9.47	6.64	- 2.42	-	-
	30 Hz	6.85	2.66	5.96	- 0.79	5.15	- 3.74	-	-
	1 Hz	189.11	145.47	153.81	51.41	128.11	13.09	120.29	- 81.23
	10 Hz	20.36	27.10	18.43	9.43	14.05	5.92	12.98	- 2.13
750	20 Hz	8.44	6.73	9.89	- 3.37	5.54	4.12	-	-
	30 Hz	10.75	- 2.44	7.76	- 1.97	6.19	- 2.53	-	-
	1 Hz	194.07	231.59	173.01	110.70	145.93	29.49	140.04	- 51.74
	10 Hz	24.88	27.64	17.10	15.85	15.14	4.00	13.35	2.08
750	20 Hz	13.29	6.65	10.87	0.45	5.28	6.22	-	-
	30 Hz	11.46	- 3.92	8.75	- 1.71	6.87	- 2.89	-	-

*Performing measurement simultaneously at large amplitudes and high frequencies was not possible

Table C.6 Differential zero strain-rate viscosity, (+) and extension (-) cycles for aligned MAE samples subject to different strain amplitudes (superimposed on pre-strain of 0.21), loading frequency, and magnetic flux density

B (mT)	Frequency	$\varepsilon_0 = 0.025$		$\varepsilon_0 = 0.05$		$\varepsilon_0 = 0.1$		$\varepsilon_0 = 0.2$	
		η'_{DZSRV_0}	$\eta'_{DLSRV_{\pm}}$	η'_{DZSRV_0}	$\eta'_{DLSRV_{\pm}}$	η'_{DZSRV_0}	$\eta'_{DLSRV_{\pm}}$	η'_{DZSRV_0}	$\eta'_{DLSRV_{\pm}}$
0	1 Hz	58.76	52.49	59.33	9.91	62.75	- 29.61	46.32	- 41
	10 Hz	8.13	7.02	7.26	2.64	7.17	- 2.52	-	-
	20 Hz	5.83	- 2.30	3.09	3.59	4.60	- 3.50	-	-
	30 Hz	3.49	- 0.01	3.21	- 1.29	3.45	- 2.76	-	-
150	1 Hz	92.61	66.79	86.97	26.74	95.96	- 53.11	66.99	- 42.19
	10 Hz	11.45	10.60	11.79	0.89	10.17	- 3.17	-	-
	20 Hz	7.98	0.47	6.63	- 0.49	3.88	2.79	-	-
	30 Hz	5.97	- 0.57	5.41	- 2.47	5.09	- 4.90	-	-
300	1 Hz	140.53	133.20	127.67	48.57	125.36	- 39.34	-	- 67.16
	10 Hz	21.58	10.61	16.19	3.65	15.32	- 7.84	102.12	-
	20 Hz	10.39	5.01	8.99	- 0.30	6.33	0.34	-	-
	30 Hz	8.68	1.49	7.98	- 4.49	7.11	- 6.31	-	-
450	1 Hz	204.45	145.87	184.90	39.69	145.97	- 30.22	129.63	- 70.83
	10 Hz	31.80	2.58	20.75	6.53	16.74	- 4.1	-	-
	20 Hz	12.83	13.63	11.51	- 0.69	8.54	- 1.90	-	-
	30 Hz	10.98	1.28	9.63	- 6.18	7.59	- 6.84	-	-
600	1 Hz	222.34	202.50	180.35	71.28	178.69	- 85.71	129.16	- 80.76
	10 Hz	28.39	23.02	24.11	3.82	19.85	- 5.37	-	-
	20 Hz	18.17	- 3.53	10.52	5.23	8.55	1.31	-	-
	30 Hz	14.08	- 1.03	9.80	- 2.27	9.25	- 7.49	-	-
750	1 Hz	218.93	229.73	212.77	88.20	178.42	- 25.51	145.93	- 57.64
	10 Hz	35.16	17.21	25.15	4.02	20.18	- 6.59	-	-
	20 Hz	17.08	12.55	13.99	- 0.01	10.00	- 1.47	-	-
	30 Hz	13.17	2.40	11.39	- 4.13	8.68	- 4.89	-	-

*Performing measurement simultaneously at large amplitudes and high frequencies was not possible

References

- Samal, S., Škodová, M., Abate, L., Blanco, I.: Magneto-rheological elastomer composites a review. *Appl. Sci.* **10**, 4899 (2020). <https://doi.org/10.3390/app10144899>
- Nadzharyan, T.A., Shamonin, M., Kramarenko, E.Y.: Theoretical modeling of magnetoactive elastomers on different scales: a State-of-the-art review. *Polymers* **14**, 4096 (2022). <https://doi.org/10.3390/polym14194096>
- Stolbov, O., Raikher, Y.: Large-scale shape transformations of a sphere made of a magnetoactive elastomer. *Polymers* **12**, 2933 (2020). <https://doi.org/10.3390/polym12122933>
- Filipcsei, G., Csetneki, I., Szilágyi, A., Zrínyi, M.: Magnetic Field-Responsive Smart Polymer Composites. In: Gong, B., Sanford, A.R., Ferguson, J.S. (eds.) *Oligomers - Polymer Composites - Molecular Imprinting*, pp. 137–189. Springer, Berlin, Heidelberg (2007)
- Moreno-Mateos, M.A., Lopez-Donaire, M.L., Hossain, M., Garcia-Gonzalez, D.: Effects of soft and hard magnetic particles on the mechanical performance of ultra-soft magnetorheological elastomers. *Smart Mater. Struct.* **31**, 065018 (2022). <https://doi.org/10.1088/1361-665X/ac6bd3>
- Becker, T.I., Stolbov, O.V., Biller, A.M., Borin, D.Y., Stolbova, O.S., Zimmermann, K., Raikher, Y.L.: Shape-programmable cantilever made of a magnetoactive elastomer of mixed content. *Smart Mater. Struct.* **31**, 105021 (2022). <https://doi.org/10.1088/1361-665X/ac8f79>

7. Imaduddin, F., Mazlan, S.A., Ubaidillah Zamzuri, H., Fatah, A.Y.A.: Testing and parametric modeling of magnetorheological valve with meandering flow path. *Nonlinear Dyn.* **85**, 287–302 (2016). <https://doi.org/10.1007/s11071-016-2684-6>
8. Dehghani, R., Khanlo, H.M., Fakhraei, J.: Active chaos control of a heavy articulated vehicle equipped with magnetorheological dampers. *Nonlinear Dyn.* **87**, 1923–1942 (2017). <https://doi.org/10.1007/s11071-016-3163-9>
9. Borin, D., Stepanov, G., Dohmen, E.: Hybrid magnetoactive elastomer with a soft matrix and mixed powder. *Arch. Appl. Mech.* **89**, 105–117 (2019). <https://doi.org/10.1007/s00419-018-1456-9>
10. Tahir, S., Usman, M., Umer, M.A.: Effect of volume fraction on shear mode properties of Fe-Co and Fe-Ni filled magneto-rheological elastomers. *Polymers* **14**, 2968 (2022). <https://doi.org/10.3390/polym14142968>
11. Vatandoost, H., Hemmatian, M., Sedaghati, R., Rakheja, S.: Effect of shape factor on compression mode dynamic properties of magnetorheological elastomers. *J. Intell. Mater. Syst. Struct.* **32**, 1678–1699 (2021). <https://doi.org/10.1177/1045389X20983921>
12. Erenchun, A., Blanco, B., Gil-Negrete, N., Wang, B., Kari, L.: Effect of lubrication on the mechanical behavior of magnetorheological elastomers in compression mode. *Polym. Testing* **111**, 107617 (2022). <https://doi.org/10.1016/j.polymertesting.2022.107617>
13. Zhang, J., Qiao, Y., Zhang, M., Zhai, P.: Magnetorheological behavior of isotropic silicone rubber-based magnetorheological elastomers under coupled static–dynamic compressive loads. *Smart Mater. Struct.* **31**, 095010 (2022). <https://doi.org/10.1088/1361-665X/ac7d24>
14. Dargahi, A., Sedaghati, R., Rakheja, S.: On the properties of magnetorheological elastomers in shear mode: Design, fabrication and characterization. *Compos. B Eng.* **159**, 269–283 (2019). <https://doi.org/10.1016/j.compositesb.2018.09.080>
15. Norouzi, M., Sajjadi Alehashem, S.M., Vatandoost, H., Ni, Y.Q., Shahmardan, M.M.: A new approach for modeling of magnetorheological elastomers. *J. Intell. Mater. Syst. Struct.* **27**, 1121–1135 (2016). <https://doi.org/10.1177/1045389X15615966>
16. Li, R., Sun, L.Z.: Viscoelastic responses of silicone-rubber-based magnetorheological elastomers under compressive and shear loadings. *J. Eng. Mater. Technol.* (2013). <https://doi.org/10.1115/1.4023839>
17. Gordaninejad, F., Wang, X., Mysore, P.: Behavior of thick magnetorheological elastomers. *J. Intell. Mater. Syst. Struct.* **23**, 1033–1039 (2012). <https://doi.org/10.1177/1045389X12448286>
18. Schubert, G., Harrison, P.: Large-strain behaviour of Magneto-Rheological Elastomers tested under uniaxial compression and tension, and pure shear deformations. *Polym. Testing* **42**, 122–134 (2015). <https://doi.org/10.1016/j.polymertesting.2015.01.008>
19. Moreno, M.A., Gonzalez-Rico, J., Lopez-Donaire, M.L., Arias, A., Garcia-Gonzalez, D.: New experimental insights into magneto-mechanical rate dependences of magnetorheological elastomers. *Compos. B Eng.* **224**, 109148 (2021). <https://doi.org/10.1016/j.compositesb.2021.109148>
20. Bastola, A.K., Hossain, M.: A review on magneto-mechanical characterizations of magnetorheological elastomers. *Compos. B Eng.* **200**, 108348 (2020). <https://doi.org/10.1016/j.compositesb.2020.108348>
21. Vatandoost, H., Rakheja, S., Sedaghati, R., Hemmatian, M.: Compensation of magnetic force of an electromagnet for compression mode characterization of magnetorheological elastomers. *IEEE Trans. Magn.* **57**, 1–14 (2021). <https://doi.org/10.1109/TMAG.2020.3036234>
22. Erenchun, A., Prieto, B., Artetxe, G., Gil-Negrete, N.: Practical design of an electromagnet for the compression characterization of magnetorheological elastomers. *Smart Mater. Struct.* **31**, 095005 (2022). <https://doi.org/10.1088/1361-665X/ac7bbe>
23. Romeis, D., Kostrov, S.A., Kramarenko, E.Y., Stepanov, G.V., Shamonin, M., Saphiannikova, M.: Magnetic-field-induced stress in confined magnetoactive elastomers. *Soft Matter* **16**, 9047–9058 (2020). <https://doi.org/10.1039/D0SM01337D>
24. Bodelot, L., Voropaieff, J.-P., Pössinger, T.: Experimental investigation of the coupled magneto-mechanical response in magnetorheological elastomers. *Exp. Mech.* **58**, 207–221 (2018). <https://doi.org/10.1007/s11340-017-0334-7>
25. Lefèvre, V., Danas, K., Lopez-Pamies, O.: A general result for the magnetoelastic response of isotropic suspensions of iron and ferrofluid particles in rubber, with applications to spherical and cylindrical specimens. *J. Mech. Phys. Solids* **107**, 343–364 (2017). <https://doi.org/10.1016/j.jmps.2017.06.017>
26. Vatandoost, H., Rakheja, S., Sedaghati, R.: Effects of iron particles' volume fraction on compression mode properties of magnetorheological elastomers. *J. Magn. Magn. Mater.* **522**, 167552 (2021). <https://doi.org/10.1016/j.jmmm.2020.167552>
27. ASTM D5992–96: Standard Guide for Dynamic Testing of Vulcanized Rubber and Rubber-Like Materials Using Vibratory Methods, (2011)
28. Ewoldt, R.H., Hosoi, A.E., McKinley, G.H.: Nonlinear viscoelastic biomaterials: meaningful characterization and engineering inspiration. *Integr. Comp. Biol.* **49**, 40–50 (2009). <https://doi.org/10.1093/icb/icp010>
29. Cho, K.S., Hyun, K., Ahn, K.H., Lee, S.J.: A geometrical interpretation of large amplitude oscillatory shear response. *J. Rheol.* **49**, 747–758 (2005). <https://doi.org/10.1122/1.1895801>
30. Ewoldt, R.H. (Randy H.): Nonlinear viscoelastic materials: bioinspired applications and new characterization measures, <https://dspace.mit.edu/handle/1721.1/49556>, (2009)
31. Ewoldt, R.H., Hosoi, A.E., McKinley, G.H.: New measures for characterizing nonlinear viscoelasticity in large amplitude oscillatory shear. *J. Rheol.* **52**, 1427–1458 (2008). <https://doi.org/10.1122/1.2970095>
32. Vatandoost, H., Hemmatian, M., Sedaghati, R., Rakheja, S.: Dynamic characterization of isotropic and anisotropic magnetorheological elastomers in the oscillatory squeeze mode superimposed on large static pre-strain. *Compos. B Eng.* **182**, 107648 (2020). <https://doi.org/10.1016/j.compositesb.2019.107648>
33. Danas, K., Kankanala, S.V., Triantafyllidis, N.: Experiments and modeling of iron-particle-filled

- magnetorheological elastomers. *J. Mech. Phys. Solids* **60**, 120–138 (2012). <https://doi.org/10.1016/j.jmps.2011.09.006>
34. Vatanidoost, H., Norouzi, M., Alehashem, S.M.S., Smoukov, S.K.: A novel phenomenological model for dynamic behavior of magnetorheological elastomers in tension–compression mode. *Smart Mater. Struct.* **26**, 065011 (2017). <https://doi.org/10.1088/1361-665X/aa6126>
 35. Kim, J.H., Ahn, K.H.: Rheological characteristics of poly(ethylene oxide) aqueous solutions under large amplitude oscillatory squeeze flow. *Korea-Aust. Rheol. J.* **24**, 257–266 (2012). <https://doi.org/10.1007/s13367-012-0032-z>
 36. Phan-Thien, N.: Squeezing flow of a viscoelastic solid. *J. Nonnewton. Fluid Mech.* **95**, 343–362 (2000). [https://doi.org/10.1016/S0377-0257\(00\)00175-0](https://doi.org/10.1016/S0377-0257(00)00175-0)
 37. Bejenariu, A.G., Rasmussen, H.K., Skov, A.L., Hassager, O., Frankaer, S.M.: Large amplitude oscillatory extension of soft polymeric networks. *Rheol. Acta* **49**, 807–814 (2010). <https://doi.org/10.1007/s00397-010-0464-7>
 38. Kim, J.H., Ahn, K.H., Lee, S.J.: Model prediction of non-symmetric normal stresses under oscillatory squeeze flow. *Korean J. Chem. Eng.* **29**, 1010–1018 (2012). <https://doi.org/10.1007/s11814-011-0277-0>
 39. Xu, Y., Tao, R., Lubineau, G.: Nonlinear viscoelasticity of pre-compressed layered polymeric composite under oscillatory compression. *Compos. Sci. Technol.* **162**, 188–197 (2018). <https://doi.org/10.1016/j.compscitech.2018.04.039>
 40. Yu, W., Wang, P., Zhou, C.: General stress decomposition in nonlinear oscillatory shear flow. *J. Rheol.* **53**, 215–238 (2009). <https://doi.org/10.1122/1.3037267>
 41. Yao, N.Y., Larsen, R.J., Weitz, D.A.: Probing nonlinear rheology with inertio-elastic oscillations. *J. Rheol.* **52**, 1013–1025 (2008). <https://doi.org/10.1122/1.2933171>
 42. Janmey, P.A., Amis, E.J., Ferry, J.D.: Rheology of fibrin clots. vi. stress relaxation, creep, and differential dynamic modulus of fine clots in large shearing deformations. *J. Rheol.* **27**, 135–153 (1983). <https://doi.org/10.1122/1.549722>
 43. Gardel, M.L., Shin, J.H., MacKintosh, F.C., Mahadevan, L., Matsudaira, P., Weitz, D.A.: Elastic behavior of cross-linked and bundled actin networks. *Science* **304**, 1301–1305 (2004). <https://doi.org/10.1126/science.1095087>
 44. ISO 4664–1: Rubber, vulcanized or thermoplastic - Determination of dynamic properties - Part 1: General guidance. Geneva: International Standards Organization, (2011)
 45. Keip, M.-A., Sridhar, A.: A variationally consistent phase-field approach for micro-magnetic domain evolution at finite deformations. *J. Mech. Phys. Solids* **125**, 805–824 (2019). <https://doi.org/10.1016/j.jmps.2018.11.012>
 46. Mukherjee, D., Bodelot, L., Danas, K.: Microstructurally-guided explicit continuum models for isotropic magnetorheological elastomers with iron particles. *Int. J. Non-Linear Mech.* **120**, 103380 (2020). <https://doi.org/10.1016/j.ijnonlinmec.2019.103380>
 47. Wang, L., Chen, Z., Jiang, L., Cheng, L.: Magneto-mechanical properties of anisotropic magnetorheological elastomers with tilt angle of magnetic chain under compression mode. *J. Magn. Magn. Mater.* **570**, 170441 (2023). <https://doi.org/10.1016/j.jmmm.2023.170441>
 48. Hyun, K., Wilhelm, M., Klein, C.O., Cho, K.S., Nam, J.G., Ahn, K.H., Lee, S.J., Ewoldt, R.H., McKinley, G.H.: A review of nonlinear oscillatory shear tests: Analysis and application of large amplitude oscillatory shear (LAOS). *Prog. Polym. Sci.* **36**, 1697–1753 (2011). <https://doi.org/10.1016/j.progpolymsci.2011.02.002>
 49. Nam, J.G., Hyun, K., Ahn, K.H., Lee, S.J.: Prediction of normal stresses under large amplitude oscillatory shear flow. *J. Nonnewton. Fluid Mech.* **150**, 1–10 (2008). <https://doi.org/10.1016/j.jnnfm.2007.10.002>
 50. Ewoldt, R.H.: Defining nonlinear rheological material functions for oscillatory shear. *J. Rheol.* **57**, 177–195 (2013). <https://doi.org/10.1122/1.4764498>
 51. Karjanto, N.: Properties of Chebyshev polynomials, <http://arxiv.org/abs/2002.01342>, (2020)
 52. Boyd, J.P.: Chebyshev and Fourier Spectral Methods, Courier Corporation, 2001. Cited on: 490
 53. Poojary, U.R., Gangadharan, K.V.: Material modeling of frequency, magnetic field and strain dependent response of magnetorheological elastomer. *J. Mater. Sci.* **56**, 15752–15766 (2021). <https://doi.org/10.1007/s10853-021-06307-0>
 54. Yu, Y., Hoshyar, A.N., Li, H., Zhang, G., Wang, W.: Nonlinear characterization of magnetorheological elastomer-based smart device for structural seismic mitigation. *Int. J. Smart Nano Mater.* **12**, 390–428 (2021). <https://doi.org/10.1080/19475411.2021.1981477>
 55. Wereley, N.M., Perez, C., Choi, Y.T.: Strain-dependent dynamic compressive properties of magnetorheological elastomeric foams. *AIP Adv.* **8**, 056721 (2018). <https://doi.org/10.1063/1.5007266>
 56. Sorokin, V.V., Ecker, E., Stepanov, G.V., Shamonin, M., Monkman, G.J., Kramarenko, E.Y., Khokhlov, A.R.: Experimental study of the magnetic field enhanced Payne effect in magnetorheological elastomers. *Soft Matter* **10**, 8765–8776 (2014). <https://doi.org/10.1039/C4SM01738B>

Publisher's Note Springer Nature remains neutral with regard to jurisdictional claims in published maps and institutional affiliations.